1-1-1975

The design and construction of a 60 Hz repetition rate pulsed nitrogen laser.

James S. Kolodzey

THE DESIGN AND CONSTRUCTION OF A 60 HZ REPETITION RATE PULSED NITROGEN LASER.

by

James S. Kolodzey

A Thesis

Presented to the Graduate Committee

in Candidacy for the Degree of

Master of Science

in

Electrical Engineering

Lehigh University

1975

This thesis is accepted and approved in partial fulfillment of the requirements for the degree of Master of Science.

May 6, 1975
(Date)

Professor in Charge

Chairman of Department

Acknowledgements

The author gratefully acknowledges the helpful advice, aid, and motivation provided by both Dr. N. Eberhardt and Dr. E. Bergmann in completing this investigation.

The author also wishes to thank his sister, Sharon Kolodzey who helped with the typing.

TABLE OF CONTENTS

List of Figures

List of Tables

Symbols

Hz	Hertz - cycles per second
N_2	Molecular Nitrogen
V	Voltage
R	Resistance
L	Inductance
C	Capacitance
t	Time
X	Reactance
S	Complex Power
P	Real Power
Q	Reactive Power
VA	Volt - Amperes
F	Farads - Capacitance
H	Henry - Inductance
m	Meter
sec	Second
	Ohms

Prefixes

M	10^{6}	m	10^{-3}
K	10^{3}	μ	10^{-6}
c	10^{-2}	n	10^{-9}

Abstract

This thesis presents the design and construction of a pulsed nitrogen laser using a high voltage power transformer as a voltage source, giving a pulse repetition rate of 60 Hz, with breakdown every cycle. The first part of the investigation concerns the computer modeling of a transformer charging an energy storage capacitance which in turn discharges into a pulse forming line. Results are compared with experimental evidence. The second part presents a theoretical model of a nitrogen laser as a spark gap terminated transmission line. The equations obtained are solved numerically on a computer and the plotted results are compared with experimental evidence in the literature. A laser, based on the above theory, is constructed and its performance measured.

Chapter 1 INTRODUCTION

This thesis presents an investigation related to pulsed nitrogen lasers operating at a 60 Hertz repetition rate. Most of the investigation covers two areas; the power supply, and the pulse forming line. For the power supply analysis, a circuit model predicting the voltage and current behavior is developed. The pulse forming line investigation is a theoretical attempt to understand the waveforms during the laser discharge.

The investigation was conducted to demonstrate the feasibility of operating nitrogen lasers at repetition rates related to the 60 Hz line frequency. This demonstration is an effort to improve the usefulness and simplicity of N_2 lasers as laboratory tools. High repetition rates can be useful because the optical output becomes quasi-continuous which means that the eye perceives a continuous output.

A high repetition rate, above 10 Hz, is an unusual operating mode for an N_2 laser. Typically a high voltage dc power supply is used to charge an energy storage capacitance through a large resistance. The resulting pulse repetition rates are at most a few Hertz. Operation at 60 Hz eliminates the need for either a dc supply or a rectifying circuit with an ac supply. A simple high voltage power transformer can be used.

The transmission line voltage and current waves which deliver energy to the laser gas are still poorly understood. To help gain insight into the waveform behavior, a theoretical investigation is carried out. The investigation consists of computer modeling the laser by a charged transmission line terminated in a spark gap. Equations were derived which treat the spark gap as a resistance that depends on the previous history.

Chapter 2 POWER SUPPLY FOR A 60 HERTZ REPETITION RATE

2.1 General Requirements

Pulsed gas laser power supplies must be capable of supplying large currents at high voltages for short durations. A capacitor discharge system is a natural way to supply the large voltages and currents. A spark gap is used to switch the capacitor energy into the laser gas in a short time. For a 60 Hz laser, high voltage transformers are suitable voltage sources for charging the capacitor. The 60 Hz power supply can also be used for other laser repetition rates. By varying the shape of the spark gap electrodes and by carefully adjusting the gap length, repetition rates of 120 Hz, 60 Hz and 30 Hz can be obtained.

This chapter describes the behavior of the transformer and associated circuity as shown in Figure 2-1. For this purpose a circuit model which gives the voltage and current waveforms will be developed.

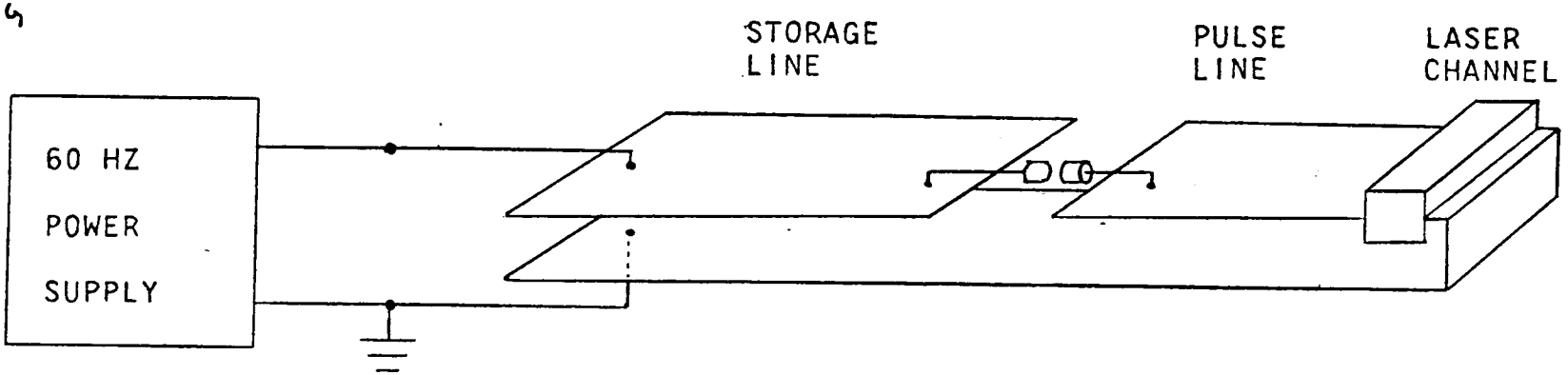

FIGURE 2-1. Capacitor Charging Circuitry.

2.2 Charging Circuit Description

The power supply circuit which charges the storage capacitor comprises a power transformer with a series inductance and resistance. This circuit, henceforth called the charging circuit, will be designed to give the laser a large output power per pulse. Required features of this circuit will now be given.

According to Godard [1], the laser output power is linearly proportional to V^2 where V is the capacitor voltage. A reasonable conclusion is that the laser power depends on the capacitor energy E (t) given by

$$E(t) = CV^2(t). \qquad (2-1)$$

The power supply will be designed to deliver a large voltage, though in practice the voltage will be limited by dielectric breakdown of the capacitance.

The circuit schematic is given in Figure 2-2. A transformer charges the capacitor through elements L and R. The resistance R protects the transformer from overload. The spark gap discharges C into the pulse forming line which is shorted by the laser channel in a time much less than 1/60 second. Therefore, for purposes of power supply design, the pulse line can be represented as a short circuit. To accurately predict the power supply behavior, a circuit model must be obtained. But first a transformer equivalent circuit is needed.

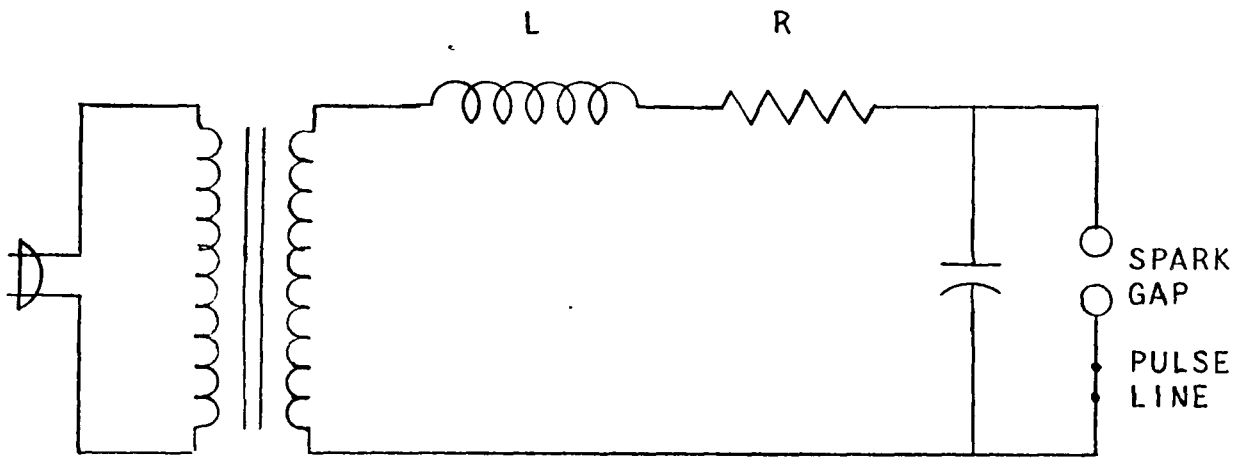

FIGURE 2-2. Charging Circuit Schematic

2.3 Transformer Equivalent Circuit

An approximate equivalent circuit for a transformer is shown in Figure 2-3, in three equivalent representations. This circuit is valid for an iron core power transformer operating at its rated frequency. At the center of the equivalent circuit is an ideal transformer. It is lossless and each coil has infinite inductance with a number of turns given by N_1, N_2, where turns ratio a is defined as

$$a = \frac{N_1}{N_2} \quad . \tag{2-2}$$

The remaining elements represent losses and leakages. Resistances R_1 and R_2 represent the non-zero resistance of the windings, and elements X_1 and X_2 are leakage inductances which result from magnetic flux escaping the core. Impedances r_1 and ωl_1 describe the exciting current which flows even without an external load. The exciting current results from hysteresis and eddy current losses in addition to the magnetizing current which magnetizes the iron core. The various circuit elements can be referred to either the primary or secondary by suitably multiplying by the turns ratio squared, a^2. For a particular transformer, the equivalent circuit elements are determined by measurement.

The power handling capability of a transformer is determined by the VA rating, explained as follows.

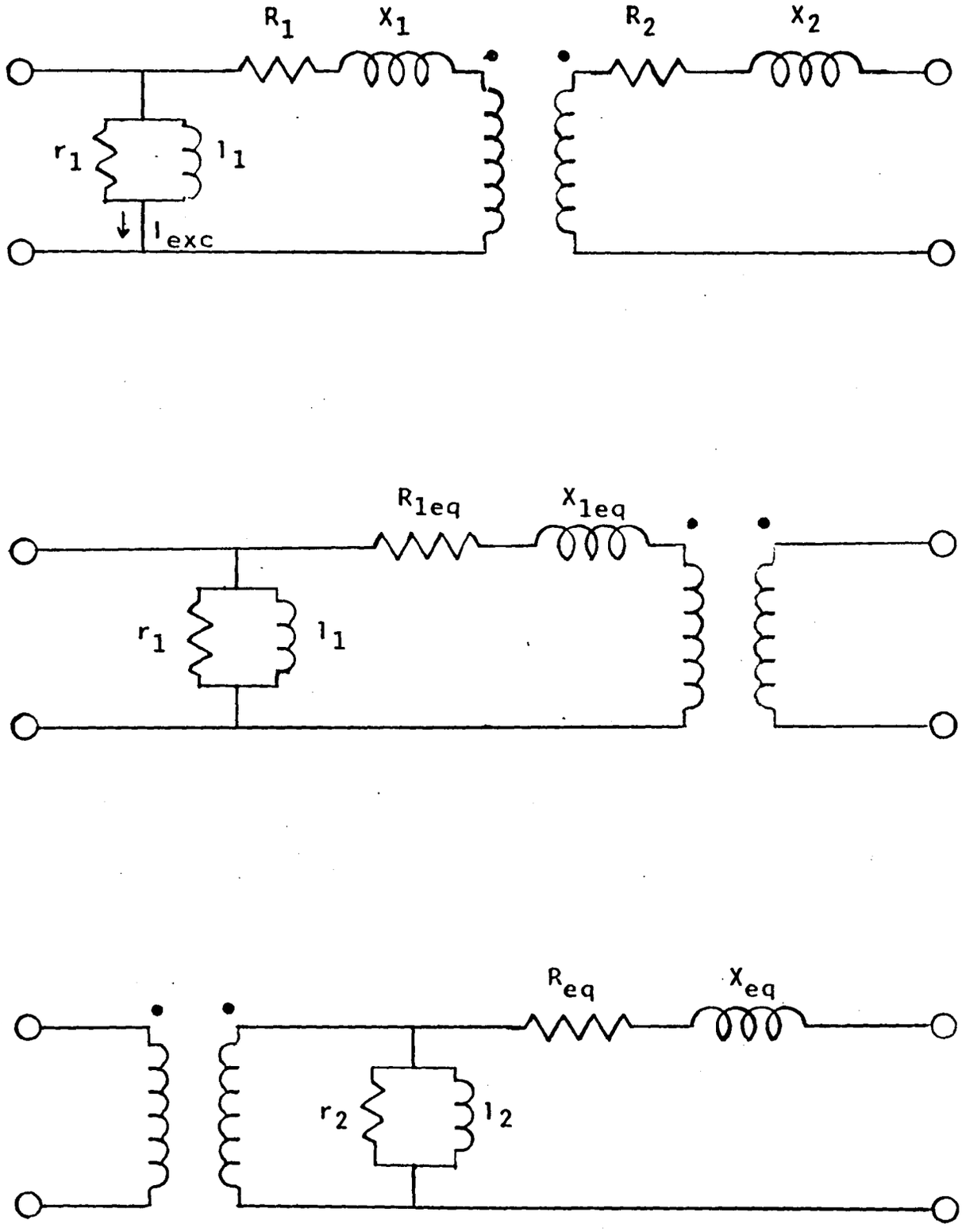

FIGURE 2-3. Transformer Equivalent Circuits.

Consider a sinusoidal excitation of a one port circuit. Using phasor notation, the voltage, V, and current, I, are

$$V(t) = V_o e^{jwt}$$
$$I(t) = I_o e^{-j\phi} e^{jwt} \qquad (2\text{-}3)$$

where V_o, I_o are real rms amplitudes. A complex power, S, delivered to the load is defined as

$$S = P + jQ = VI^* = V_o I_o e^{j\phi} = V_o I_o (\cos\phi + j\sin\phi). \qquad (2\text{-}4)$$

All variables used throughout this thesis are in rms amplitudes unless otherwise stated. The real part of S, $V_o I_o \cos\phi$, is the average power dissipated in the load, measured in watts. The imaginary part, $V_o I_o \sin\phi$, is the reactive power, representing the rms amplitude of the time varying component of instantaneous power, measured in vars (Volt-Amperes-Reactive). The magnitude of S is

$$ISI = \sqrt{P^2 + Q^2} = V_o I_o \qquad (2\text{-}5)$$

with units of VA (Volt Amperes).

The VA limit, ISI, can be used to define a maximum permissible load current, I_m. Using equation (2-5) and the transformer open circuit voltage V_{oc}, I_m is given by

$$I_m = \frac{ISI}{V_{oc}} . \qquad (2\text{-}6)$$

This current limit is maintained by choosing an appropriate external series resistance, R_s, as in Figure 2-4.

The above analysis will now be applied to a particualr transformer. The transformer is a Thordarson type 2470. Primary voltage is 110 VAC and the secondary is 25 KVAC with a corresponding turns ratio, a, given by

$$a = \frac{N_1}{N_2} = 4.4 \cdot 10^{-3} = \frac{1}{226} \qquad (2\text{-}7)$$

The power rating, ISI, is 1,000 VA. Measurement of the equivalent circuit is straightforward and is described in Appendix A. The results are included in Figure 2-5.

Note that the large exciting impedances, r_2 and l_2 are in parallel with an ideal source and so do not affect the charging circuit operation. These exciting elements will henceforth be neglected.

Equation (2-6) is now used to calculate the load current limit:

$$I_m = \frac{ISI}{V_{oc}} = \frac{1000\ VA}{25\ KV} = .04\ Amp. \qquad (2\text{-}8)$$

This value is an important design parameter.

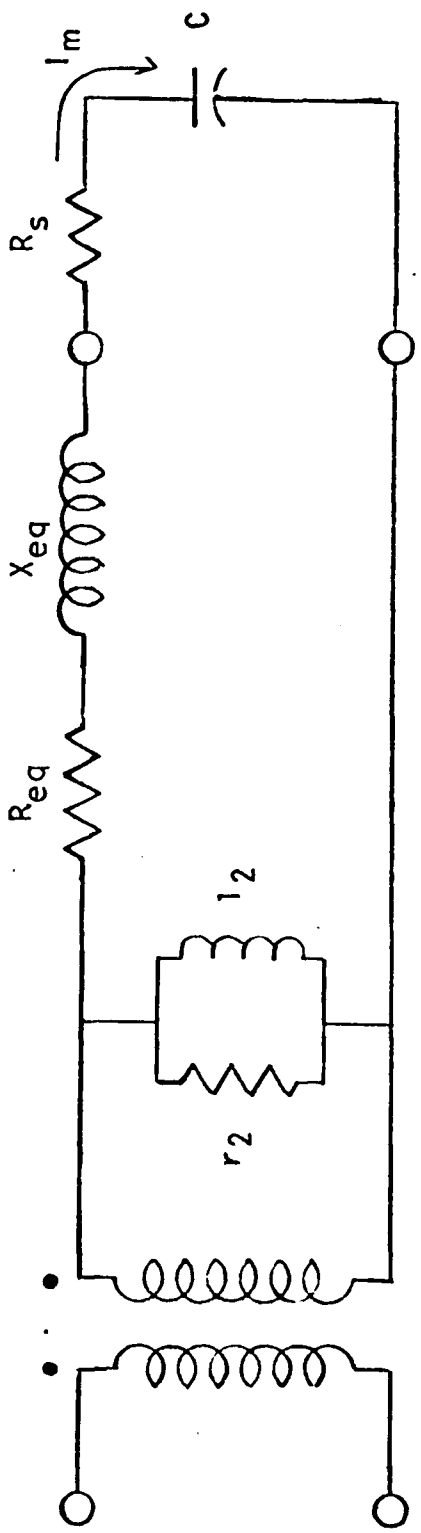

FIGURE 2-4. Transformer with External Circuitry.

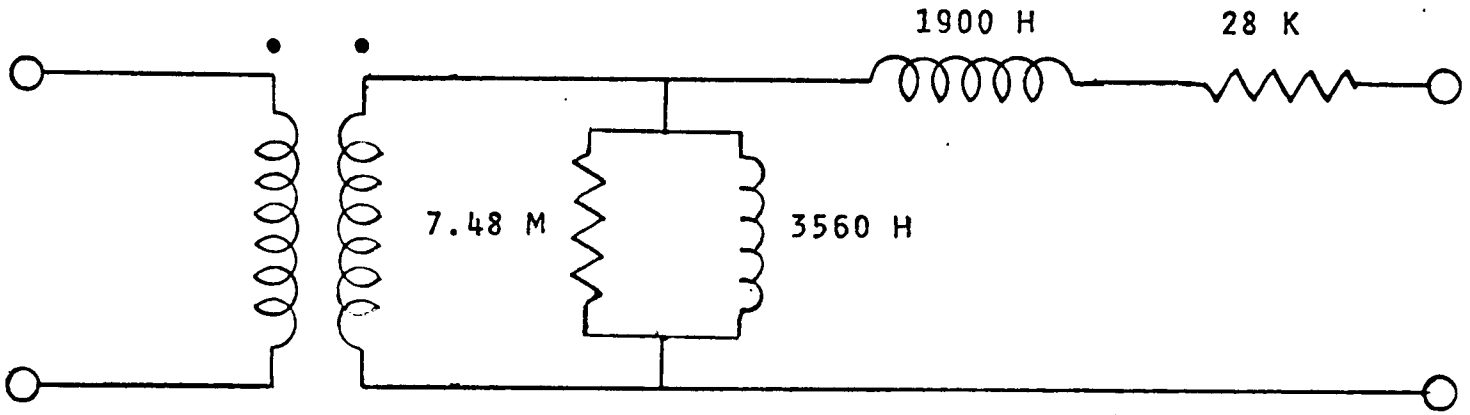

FIGURE 2-5. Transformer Measurement Results.

2.4 Final Circuit and Computer Analysis

The charging circuit in final form is shown in Figure 2-6. When the voltage across C reaches the spark gap firing voltage, the capacitor rapidly discharges into the pulse line. The residual resistance of the spark gap is much less than one ohm, and with C in the nanofarad range, the associated discharge time constant is roughly

$$\tau_d = RC \approx 1 \times 1 \cdot 10^{-9} = 1\ nsec \qquad (2\text{-}9)$$

This time is almost instantaneous compared to the 60 Hz period of 16.7 msec.

Oscillograms of the capacitor voltage and current wave forms with and without spark gap breakdown are shown in Figures 2-7 and 2-8. A total resistance of 600 KΩ, a capacitance of 2.5 nF and a repetition rate of 30 Hz was used for these photos. Note that at breakdown the voltage drops abruptly, as expected, and that the current changes only slightly. These facts are useful for the development of a mathematical model.

A rigorous model for the circuit is very difficult to obtain because of the nonlinear spark gap. However, this nonlinear behavior occurs only during spark gap breakdown. Otherwise the circuit is a linear RLC series circuit so during most of the time a linear approach can be used.

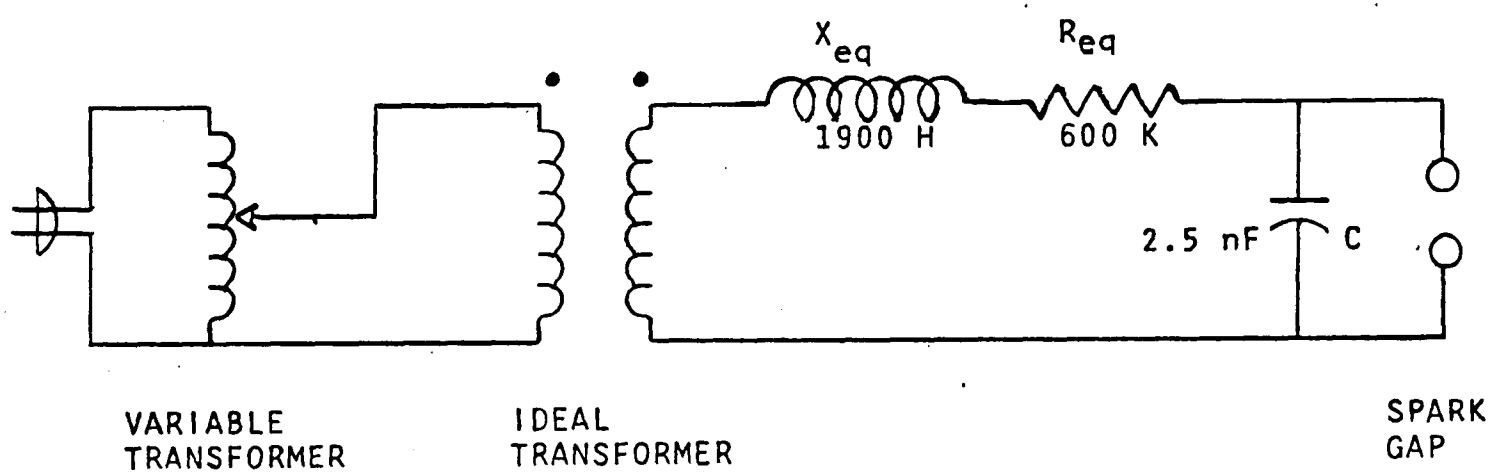

FIGURE 2-6. Final Charging Circuit.

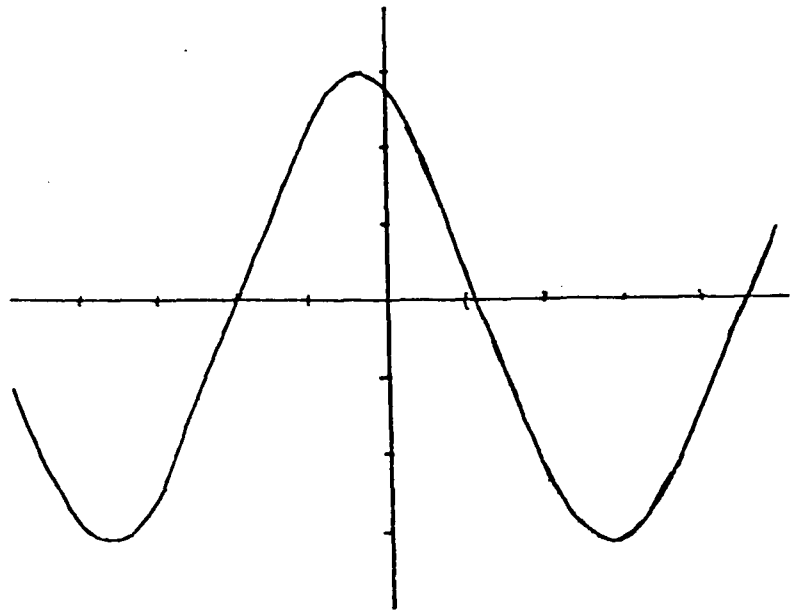

a). Without Breakdown.

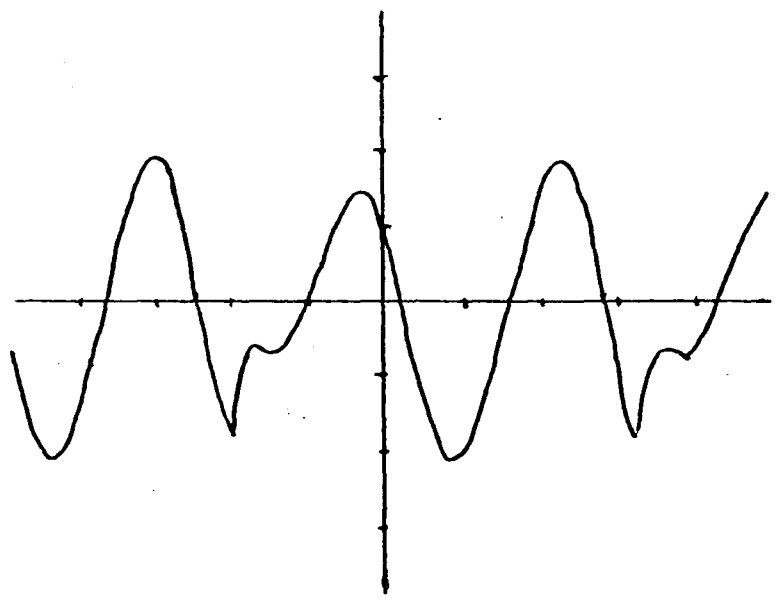

b). With Breakdown.

FIGURE 2-7. Voltage Oscillograms (60 Hz).

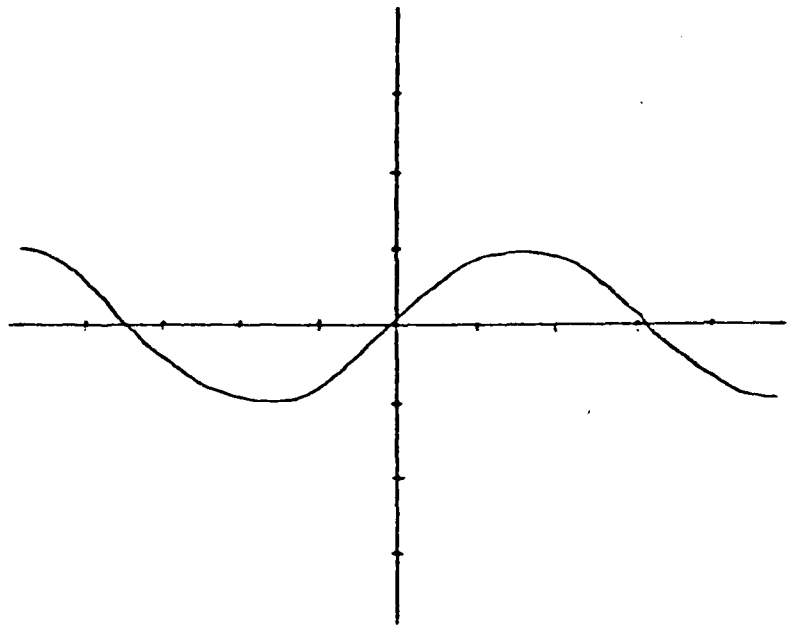

a). Without Breakdown.

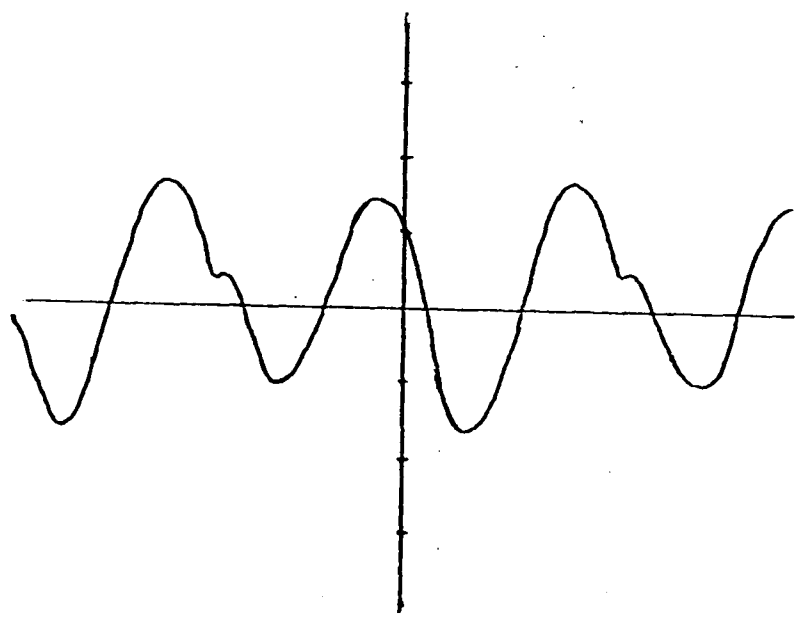

b). With Breakdown.

FIGURE 2-8. Current Oscillograms.

To develop the model, three assumptions are made. Firstly, breakdown occurs instantaneously; this is reasonable by equation (2-9). Secondly, the current through L_{eq}, being the integral over voltage, is continuous; as supported by Figure 2-8. Thirdly, the capacitor voltage drops instantaneously to a near zero residual value as supported by Figure 2-7. Altogether, the operation of the circuit has to be understood as follows: after an abrupt breakdown, the capacitor begins recharging with initial conditions determined by the second and third assumptions given above. Between spark gap breakdowns, the charging is described by the linear equations derived in Appendix B, and stated below. These equations give both the transient and steady state response for the capacitor voltage and current with arbitary initial conditions.

The capacitor voltage is

$$v_c(t) = \omega_o^2 V_s e^{-\alpha t}\left\{\left[\frac{(\alpha^2 - \omega_d^2 + \omega^2)\sin\omega_d t + 2\alpha\omega_d\cos\omega_d t}{(\alpha^2 - \omega_d^2 + \omega^2)^2 + 4\alpha^2\omega_d^2}\right]\right.$$

$$\times\left(\frac{\omega}{\omega_d}\cos\phi - \frac{\alpha}{\omega_d}\sin\phi\right)$$

$$\left. + \sin\phi\left[\frac{(\alpha^2 - \omega_d^2 + \omega^2)\cos\omega_d t - 2\alpha\omega_d\sin\omega_d t}{(\alpha^2 - \omega_d^2 + \omega^2)^2 + 4\alpha^2\omega_d^2}\right]\right\}$$

$$+ \frac{\omega_o^2 V_s \cos\phi \sin(\omega t - \psi_1)}{\left[(\omega_o^2 - \omega^2)^2 + 4\alpha^2\omega^2\right]^{1/2}}$$

$$+ \frac{\omega_o^2 V_s \sin\phi \sin(\omega t + \psi_2)}{\left[(\alpha^2 - \omega_d^2 + \omega^2)^2 + 4\alpha^2\omega_d^2\right]^{1/2}}$$

$$+ V_{co}\frac{\omega_o}{\omega_d}e^{-\alpha t}\cos(\omega_d t - \theta)$$

$$+ \frac{I_o}{\omega_d C}e^{-\alpha t}\sin\omega_d t \quad .$$

(2-10)

The current is given by

$$i_c(t) = \omega_o^2 C V_s e^{-\alpha t}\left\{\left[\frac{(\omega/\omega_d)\cos\phi - (\alpha/\omega_d)\sin\phi}{(\alpha^2-\omega_d^2+\omega^2)^2+4\alpha^2\omega_d^2}\right]\right.$$

$$\times\left[\omega_d(\omega^2-\alpha^2-\omega_d^2)\cos\omega_d t - \alpha(\alpha^2+\omega_d^2+\omega^2)\sin\omega_d t\right]$$

$$-\frac{\sin\phi}{(\alpha^2-\omega_d^2+\omega^2)^2+4\alpha^2\omega_d^2}\left[\alpha(\alpha^2+\omega_d^2+\omega^2)\cos\omega_d t\right.$$

$$\left.\left.+\omega_d(\omega^2-\alpha^2-\omega_d^2)\sin\omega_d t\right]\right\}$$

$$+\frac{\omega\omega_o^2 C V_s\cos\phi\cos(\omega t-\psi_1)}{\left[(\omega_o^2-\omega^2)^2+4\alpha^2\omega^2\right]^{1/2}}$$

$$+\frac{\omega\omega_o^2 C V_s\sin\phi\cos(\omega t+\psi_2)}{\left[(\alpha^2-\omega_d^2+\omega^2)^2+4\alpha^2\omega_d^2\right]^{1/2}}$$

$$-\omega_o C V_{co} e^{-\alpha t}\left[\frac{\alpha}{\omega_d}\cos(\omega_d t-\theta)+\sin(\omega_d t-\theta)\right]$$

$$+I_o e^{-\alpha t}\left[\cos\omega_d t-\frac{\alpha}{\omega_d}\sin\omega_d t\right] . \qquad (2\text{-}11)$$

For both equations the following definitions were used,

$v_s(t) = V_s \sin(\omega t + \phi)$ = Driving voltage,

V_{co} = initial capacitor voltage,

I_o = initial series current,

$\psi_1 = \tan^{-1}\left\{\frac{2\alpha\omega}{\omega_o^2 - \omega^2}\right\}$

$\psi_2 = \tan^{-1}\left\{\frac{\omega_o^2 - \omega^2}{2\alpha\omega}\right\}$

$\theta = \tan^{-1}\{\alpha/\omega_d\}$

$\alpha = R/2L$ = damping constant,

$\omega_o = 1/\sqrt{LC}$ = resonant frequency,

$\omega_d = \sqrt{\omega_o^2 - \alpha^2}$ = characteristic frequency,

ω = source frequency

V_s = source voltage amplitude,

ϕ = source phase.

The total circuit response including spark gap effects is obtained by repeatedly solving the equations with new initial conditions after each spark gap breakdown. This iterative method is intractable without the use of a computer. A CDC 6400 Computer was used to plot these equations and the results are given in Figures 2-9 and 2-10. The plots can be compared with the oscillograms of Figures 2-7 and 2-8. The close agreement supports the validity of the computer model. A block diagram of the computer program is given in Figure 2-11. This program, written in the Fortran language, is available from Dr. N. Eberhardt with the Department of Electrical Engineering at Lehigh University, Bethlehem, Pennsylvania.

without breakdown (vert. scale: ×10,000 v.)

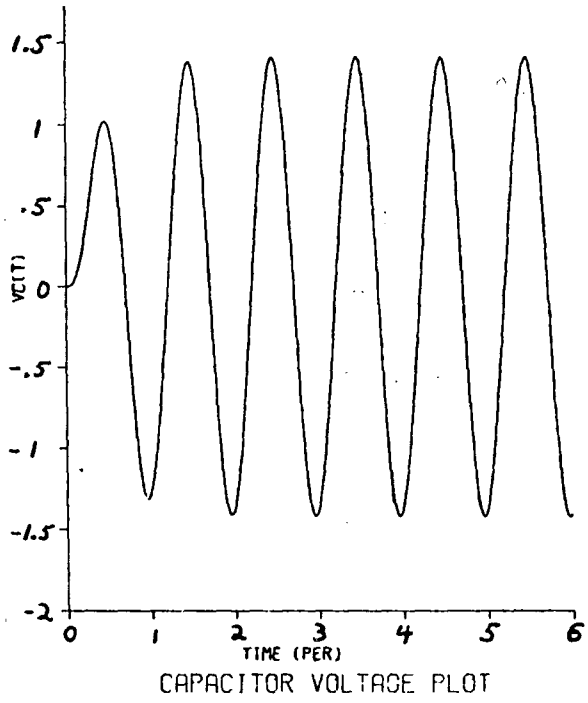

Horizontal Scales: 16.7 millisec per div.

with breakdown (vert. scale: ×10,000 v.)

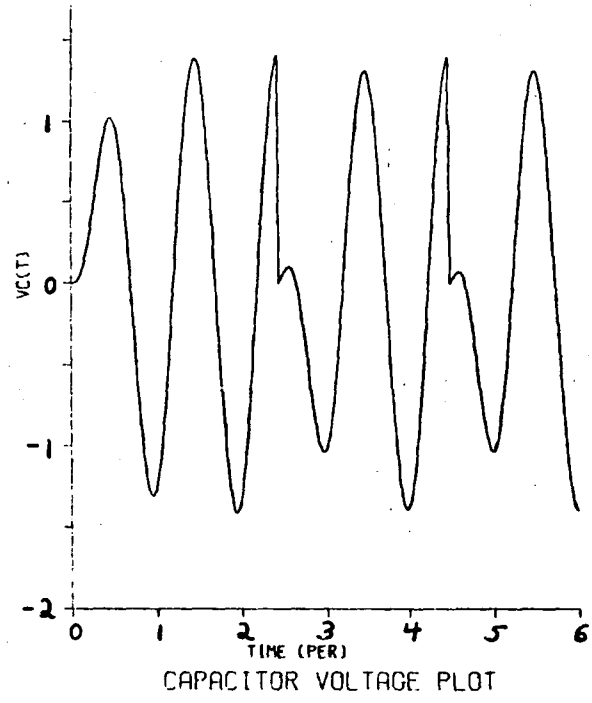

FIGURE 2-9. Computer Voltage Plot.

without breakdown (vert. scale: Amperes)

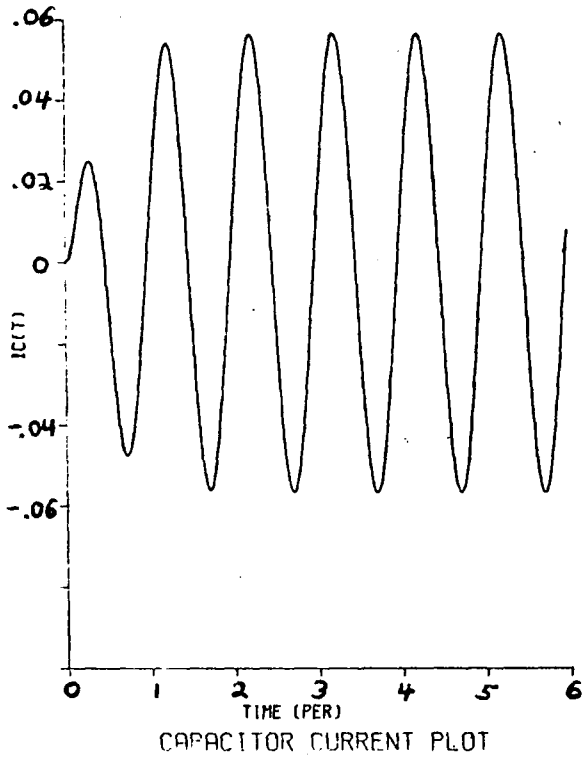

Horizontal Scales: 16.7 millisec per div.

with breakdown (vert. scale: Amperes)

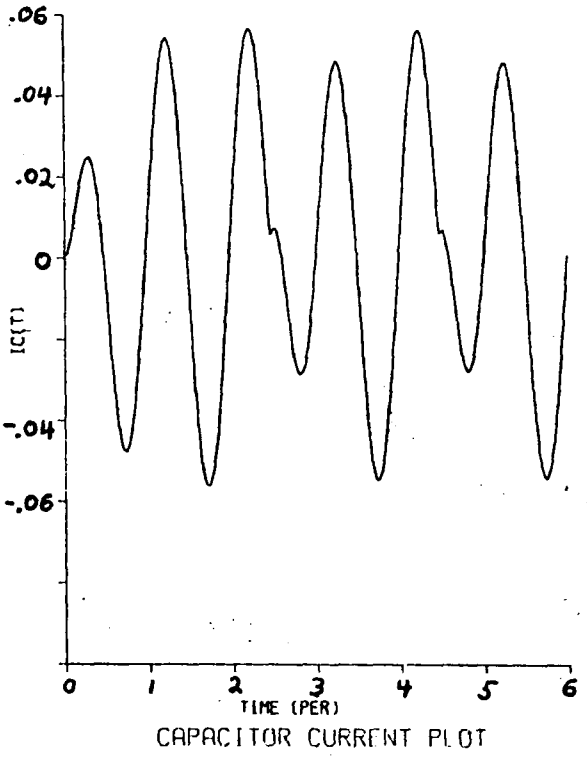

FIGURE 2-10. Computer Current Plot.

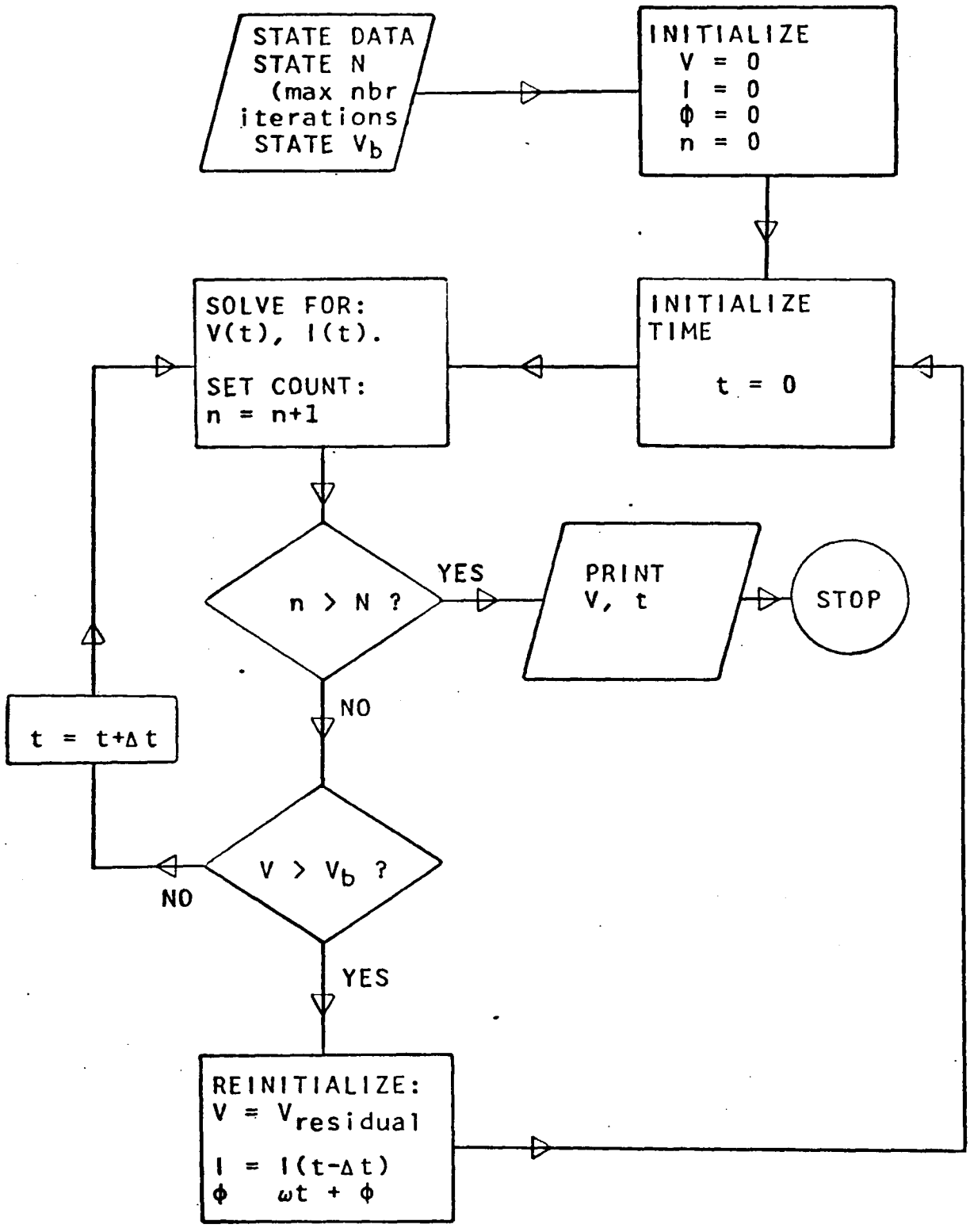

FIGURE 2-11. Block Diagram of Charging Circuit Computer Program.

2.5 Steady State Approximation

As will be shown now, some aspects of the circuit behavior can be approximated by sinusoidal steady state analysis. By this approximate method, useful design relations can be obtained which describe the voltage, current and stored energy.

The approximation is based on the computer plots in Figures 2-12, 2-13, and 2-14, and also the oscillogram of Figure 2-15. The computer plots show voltage, current and power waveforms with breakdown superimposed on the same waveforms without breakdown. Note that for each point in time the instantaneous values with breakdown are less than or equal to the value without breakdown. Therefore, it follows from the definition of rms amplitudes over an interval (t_1, t_2),

$$y_{rms} = \left[\frac{1}{(t_2 - t_1)} \int_{t_1}^{t_2} y^2(t)\, dt \right]^{1/2} \qquad (2\text{-}12)$$

that the breakdown rms value is less than or equal to the steady state rms value. This result is experimentally verified by the oscillogram of Figure 2-15. This photograph shows a plot of V on the y axis vs. I on the x axis giving two complete cycles. The outer ellipse representing sinusoidal steady state completely encloses the inner breakdown waveform. Note that here breakdown occurs only once during two cycles giving a repetition rate of 30 Hz.

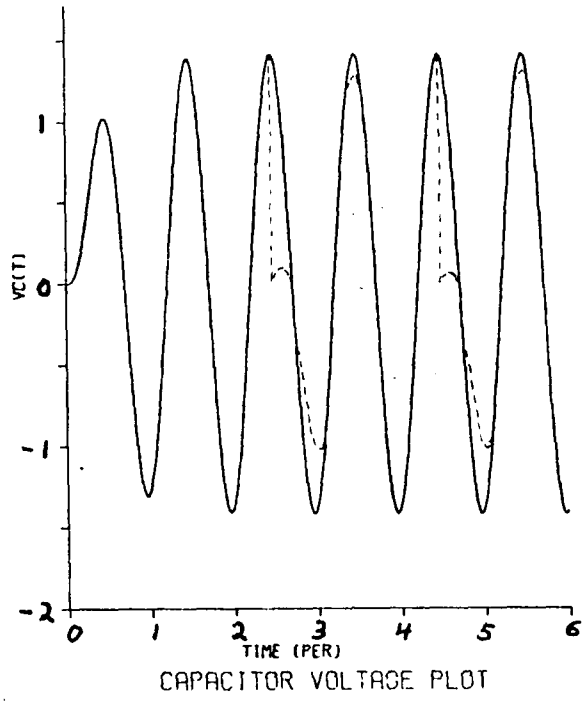

FIGURE 2-12. Superposition of Voltage Waveforms.

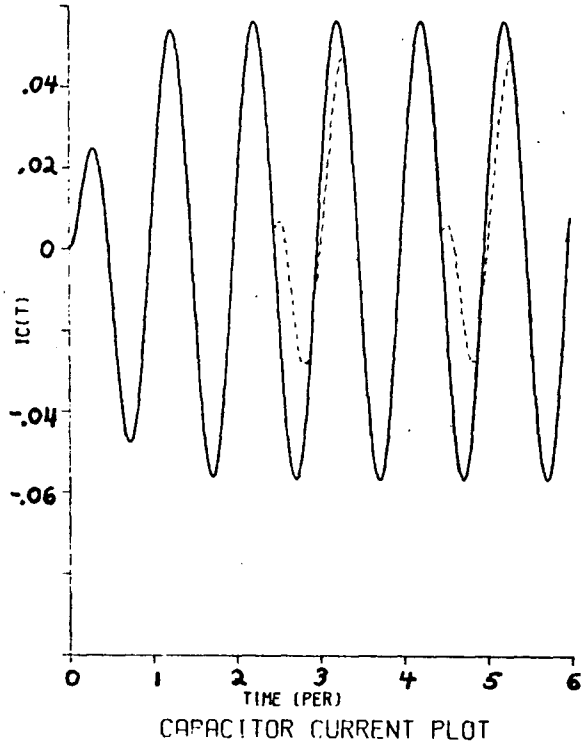

FIGURE 2-13. Superposition of Current Waveforms.

(_____)without breakdown
(----) with breakdown

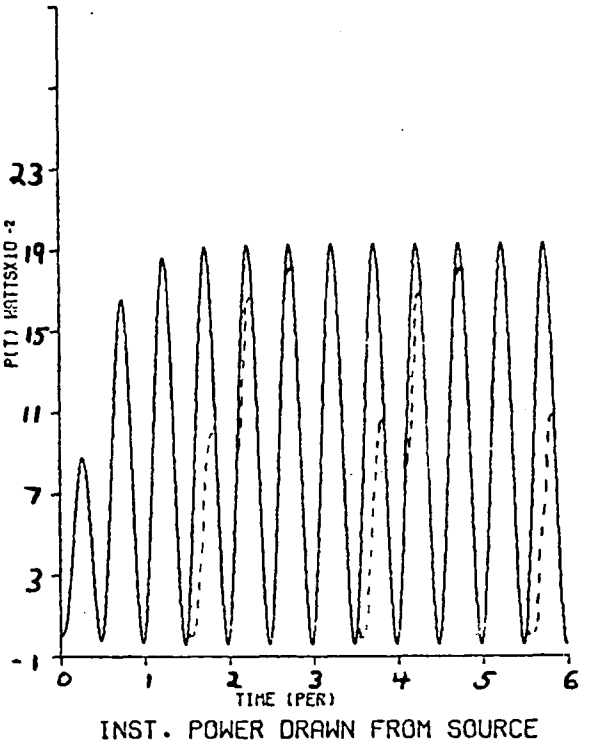

FIGURE 2-14. Superposition of Power Waveforms.

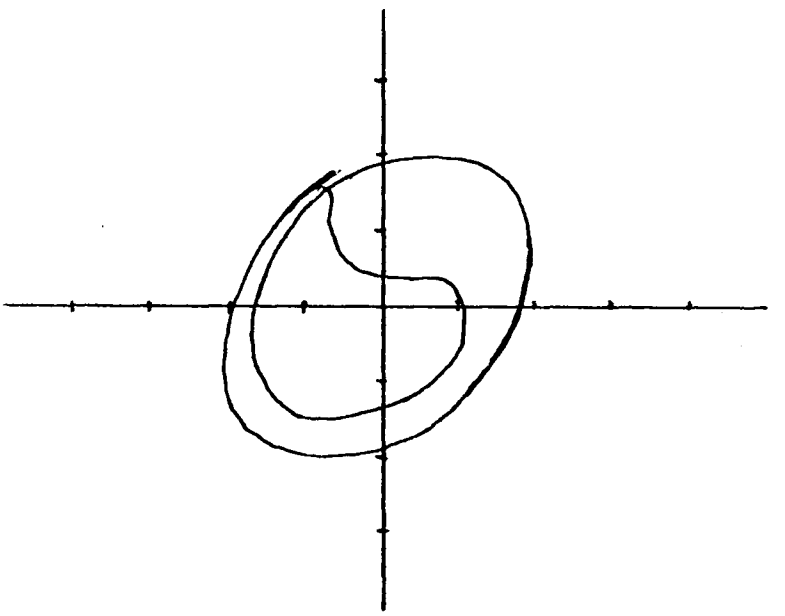

FIGURE 2-15. Oscillogram of Capacitor I-V Traces.

This steady state approach can be used to determine a value for the series resistance, R. Since in steady state the current is slightly larger, the chosen value of R will be overestimated; a smaller value could be safely used. Given the maximum permissible current, Im, determined by equation (2-8) the circuit of Figure 2-16 gives

$$R = \left[\left(\frac{V_s}{I_m}\right)^2 - \left(\omega L - \frac{1}{\omega C}\right)^2 \right]^{1/2} \tag{2-13}$$

Note that R = Req + Rs where Rs is the external resistance to be added and Req is given in Figure 2-5.

Similarly, steady state analysis gives the capacitor voltage. Again from Figure 2-16

$$V_c = \frac{I_m}{\omega C} \tag{2-14}$$

The peak stored energy becomes

$$E_s = C V_{c\,PEAK}^2 = \frac{2 I_m^2}{\omega^2 C} \tag{2-15}$$

where the factor of 2 is needed because Im is an rms quantity, whereas Es is a peak quantity. Another useful steady state quantity is the circuit efficiency, η . This quantity is defined as

$$\eta = \frac{\omega E_s}{P_{diss}} = \frac{\omega 2 I_m^2 / \omega^2 C}{2 R I_m^2} = \frac{1}{\omega R C} \tag{2-16}$$

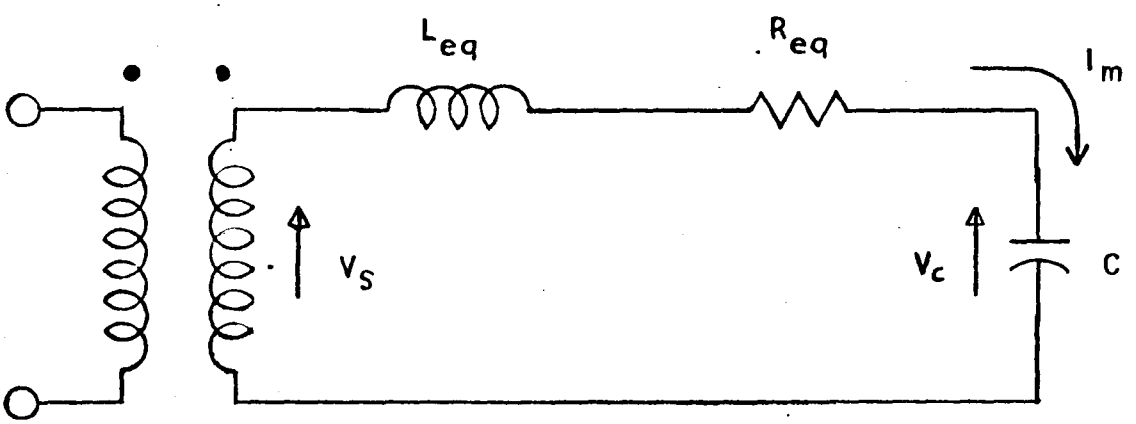

FIGURE 2-16. Charging Circuit Schematic.

The quantity, η , is a ratio of the stored capacitor energy to the power dissipated in the series resistance R. It should not be confused with the series resonator Q = wL/R.

2.6 Design Curves

The steady state design equations, described in Section 2.5, were plotted for a range of numerical values using a Hewlett Packard 9000 series Calculator. For easy comparison of the curves, C is used throughout as the independent variable on the x-axis, and the operating point, P, is labeled.

Figures 2-17, 2-18, and 2-19 show R as a function of C, L, and Im (the current limit) given by

$$R = \left[\left(\frac{V_s}{I_m}\right)^2 - \left(\omega L - \frac{1}{\omega C}\right)^2 \right]^{1/2} . \qquad (2\text{-}17)$$

Im is the contour variable and a new plot is made for each of three values of L, namely 1700 H, 1900 H and 2100 H. Figure 2-16 shows the operating point where C = 2.63 nF, L = 1900 H and R = 580 KΩ, giving Im = 40 mA.

The next graph, Figure 2-20, plots the capacitor voltage

$$V_c = \frac{I_m}{\omega C} \qquad (2\text{-}18)$$

where again Im is the contour variable. For the chosen value of C, V_c = 40 KV; this is much higher than the transformer voltage because the values of L, C are near 60 Hz resonance:

$$f_o = \frac{1}{2\pi\sqrt{LC}} = 72 \text{ Hz} . \qquad (2\text{-}19)$$

Figure 2-21 is a plot of the peak stored energy

$$E_s = \frac{2 I_m^2}{\omega^2 C} \quad . \tag{2-20}$$

The operating point shows Es = 8.7 joules.

Circuit efficiency, η ,

$$\eta = \frac{1}{\omega R C} \tag{2-21}$$

is plotted in Figure 2-22, and shows an operating value of η = 1.8. This quantity is useful for comparing the behavior of different circuits.

A brief inspection of the preceding six figures seems to indicate that a small capacitance gives the best results, in terms of voltage, stored energy and efficiency. This is true only up to a point. The capacitance value is fixed by the laser requirements, particularly the current pulse duration. However, when designing a laser cavity, the capacitances should not be made larger than necessary.

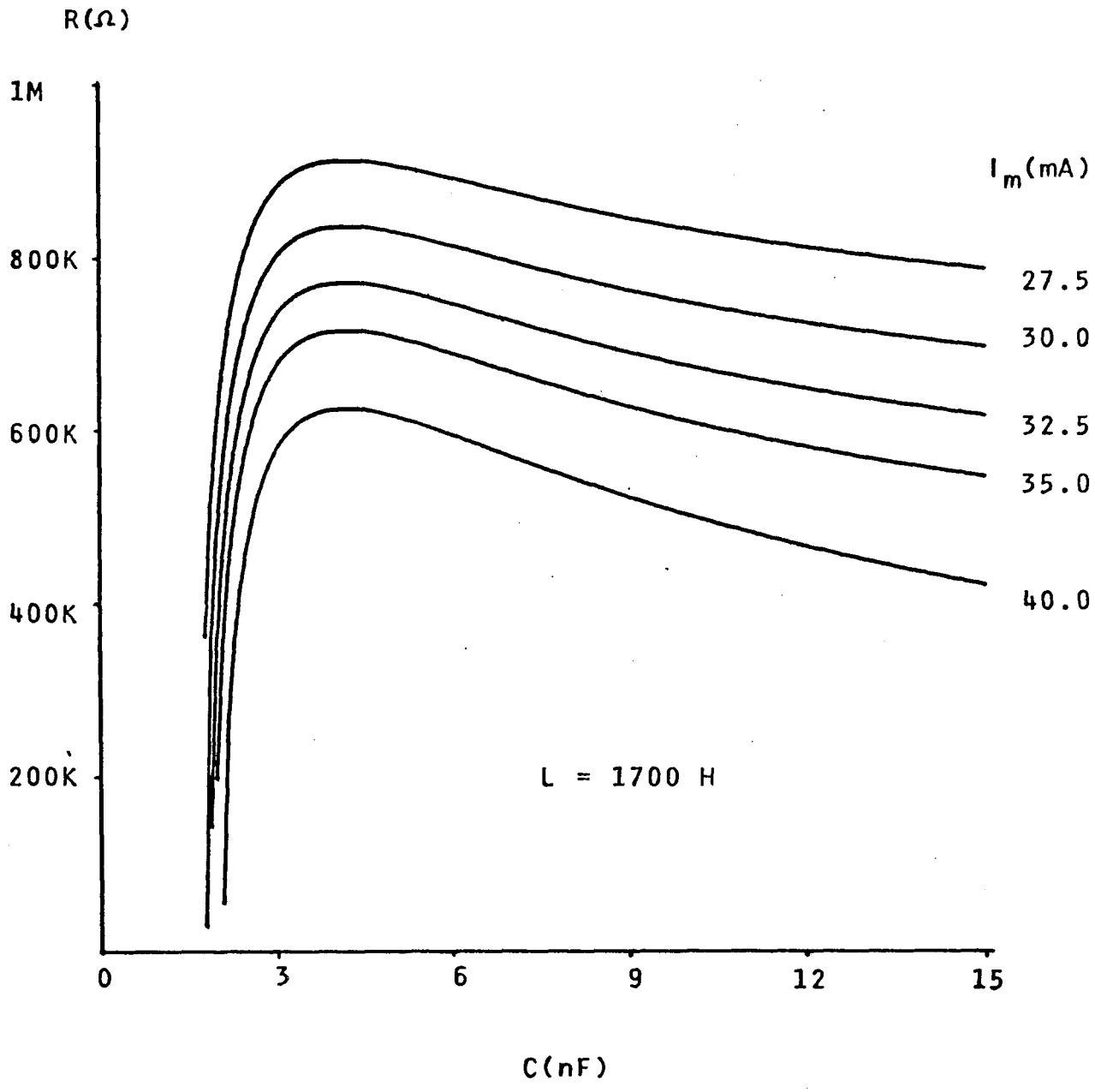

FIGURE 2-17. Resistance Design Curve.

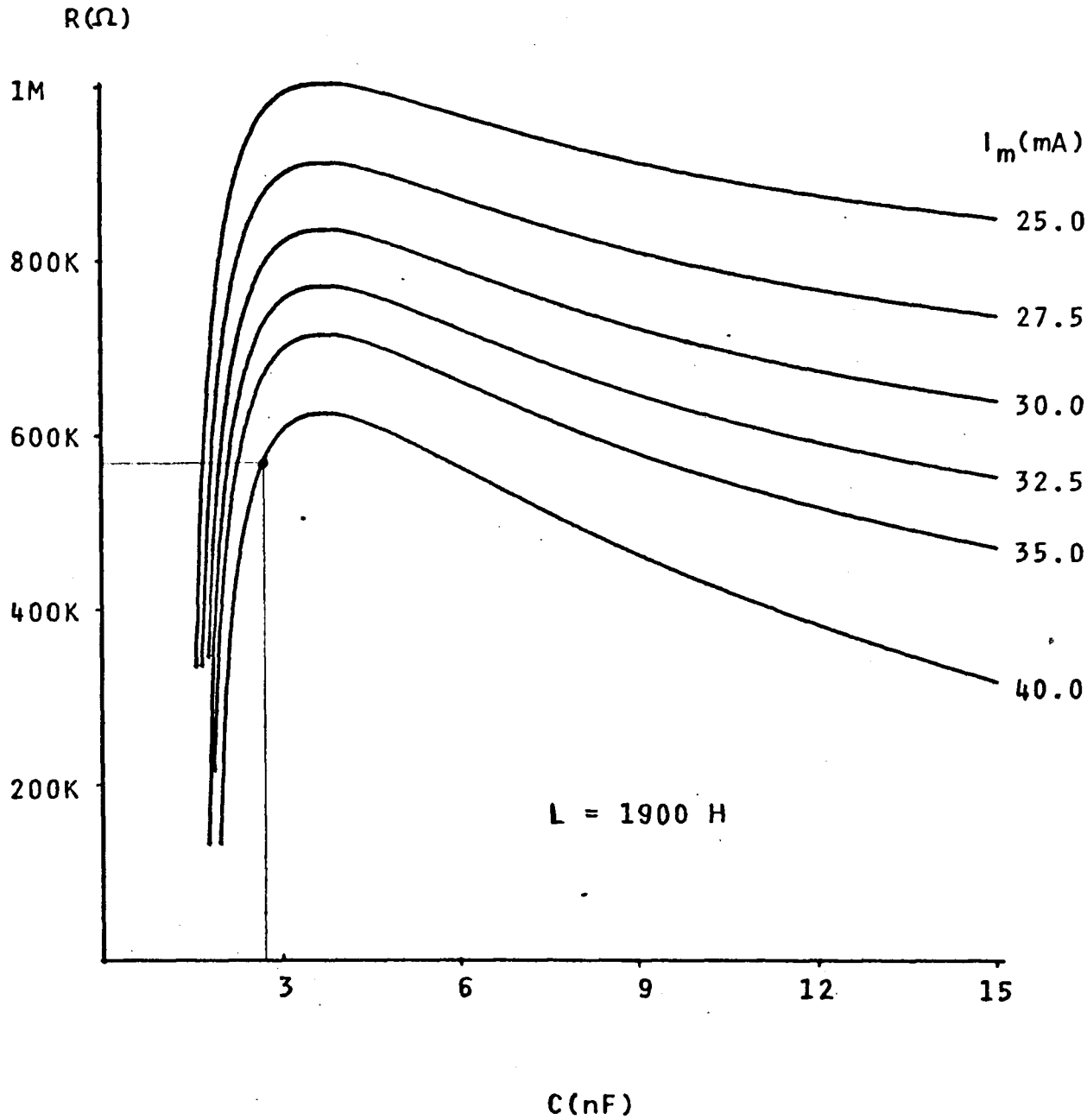

FIGURE 2-18. Resistance Design Curve.

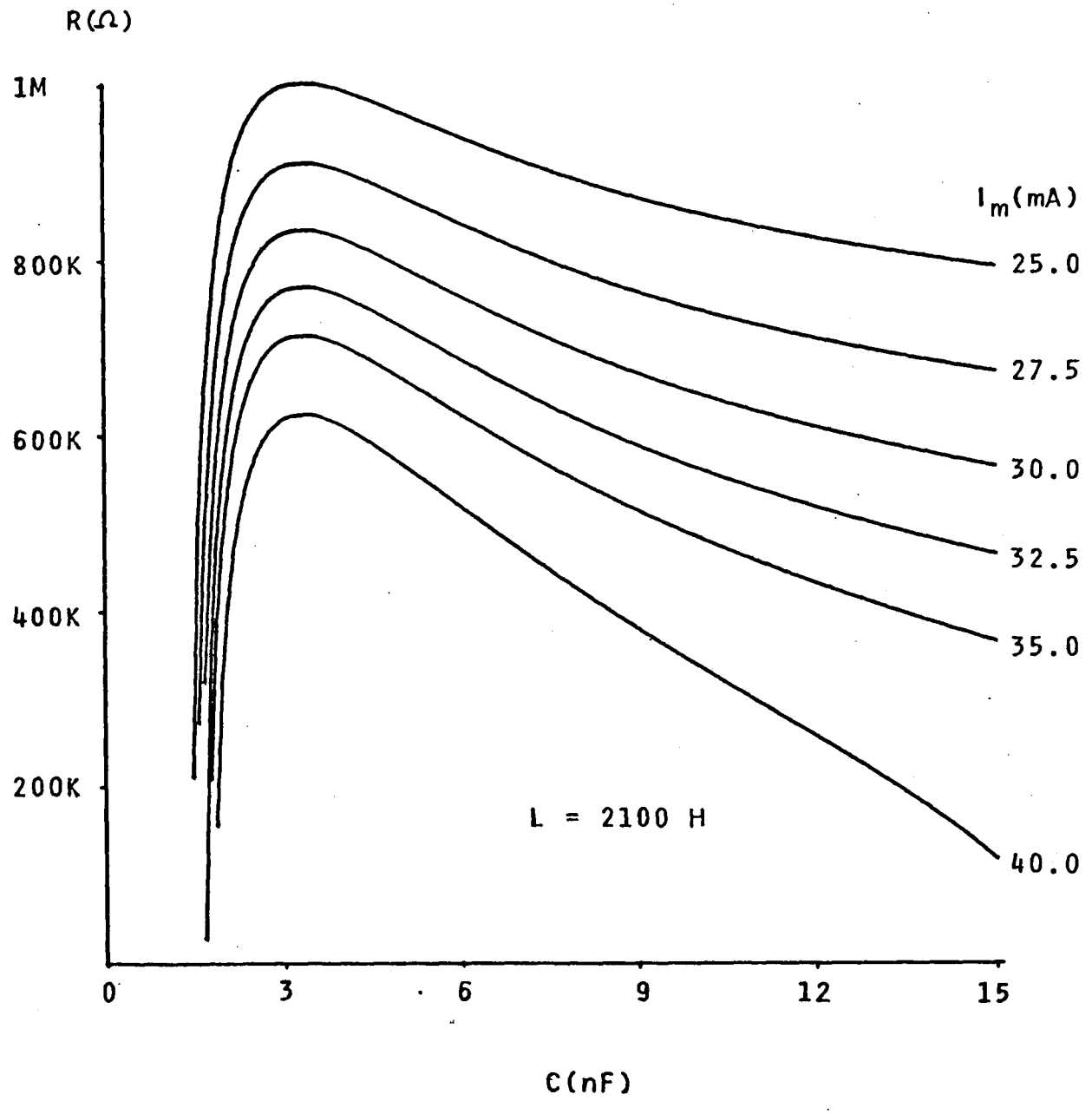

FIGURE 2-19. Resistance Design Curve.

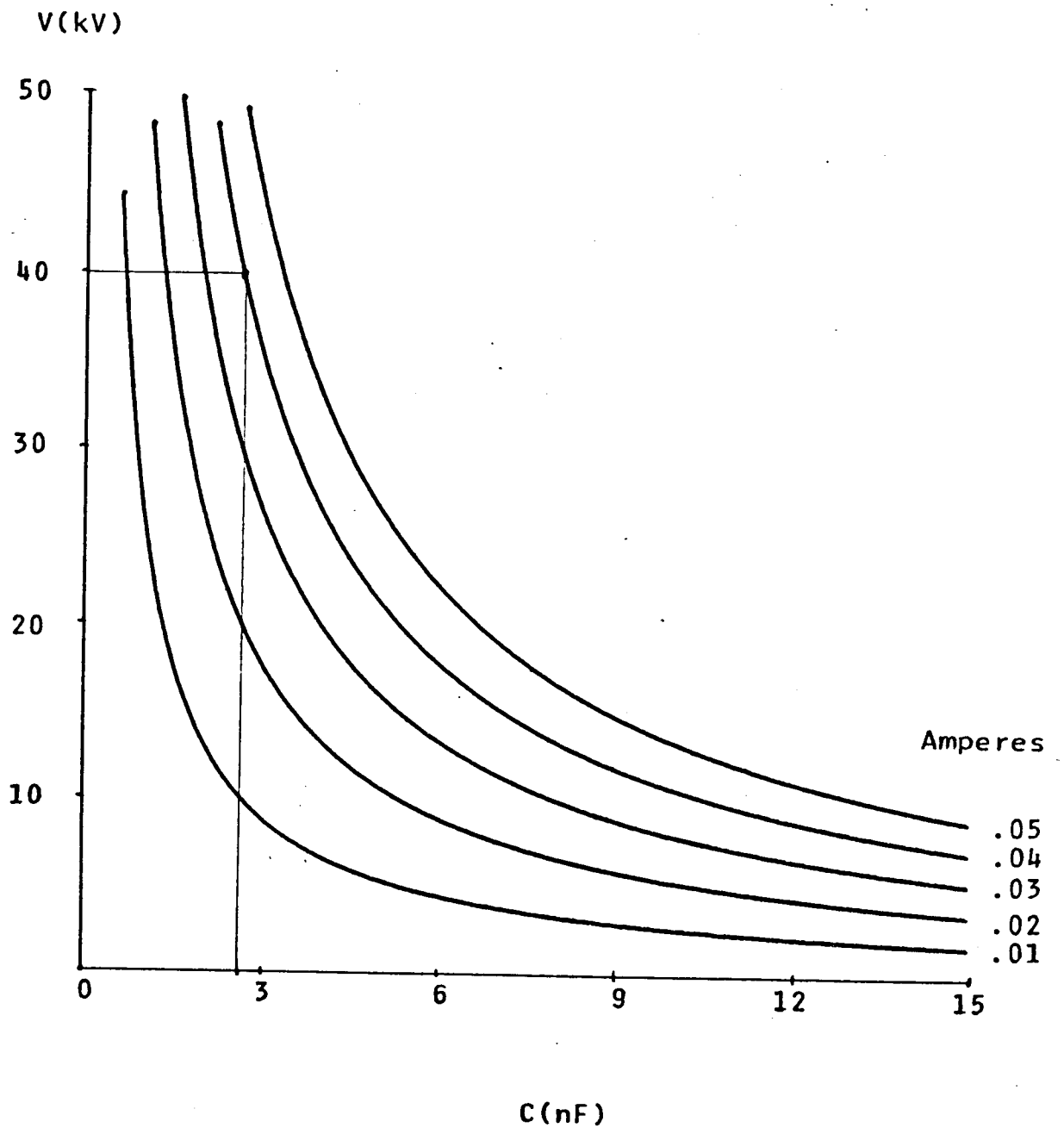

FIGURE 2-20. Capacitor Voltage Design Curve.

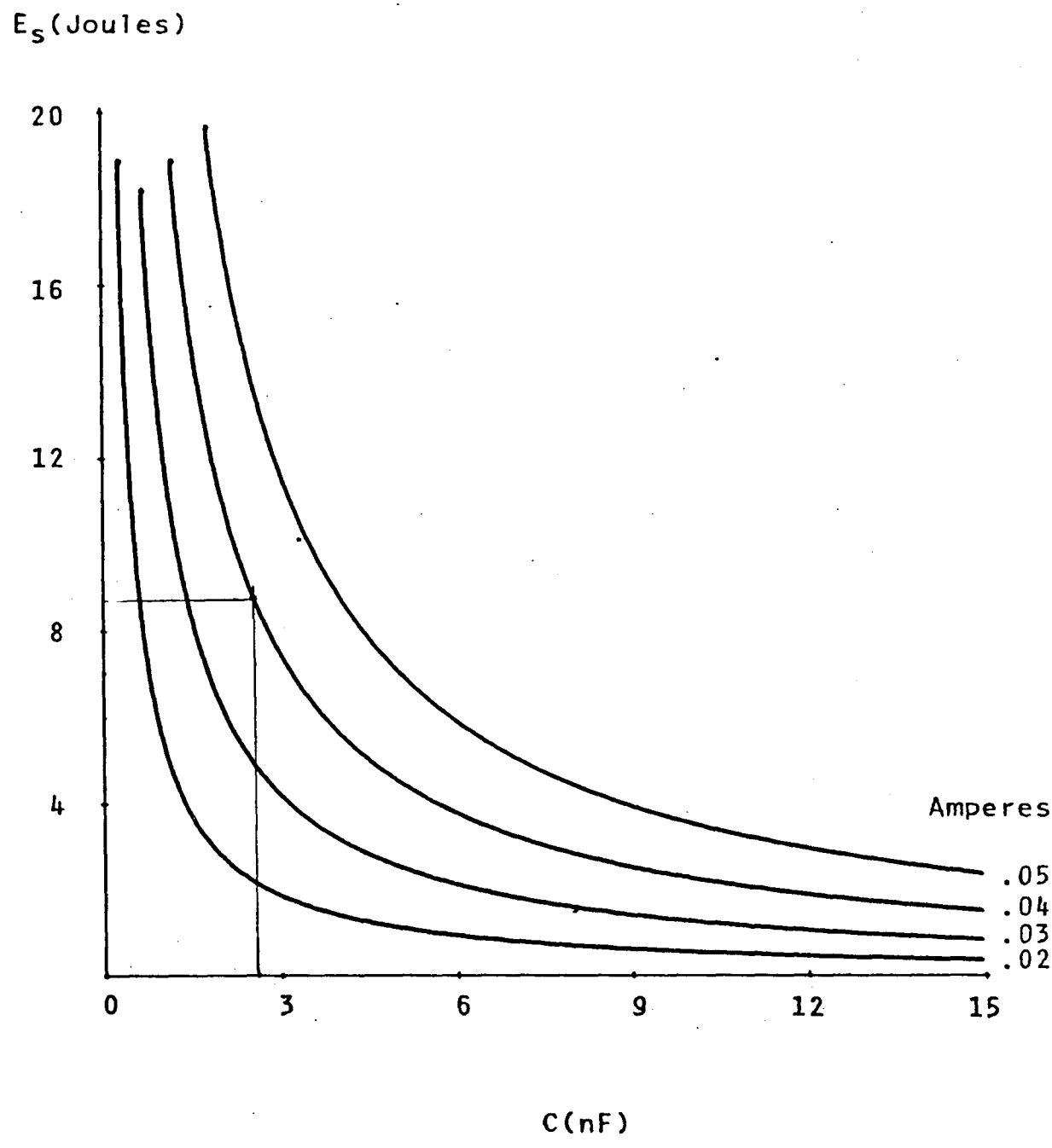

FIGURE 2-21. Peak Stored Energy Design Curve.

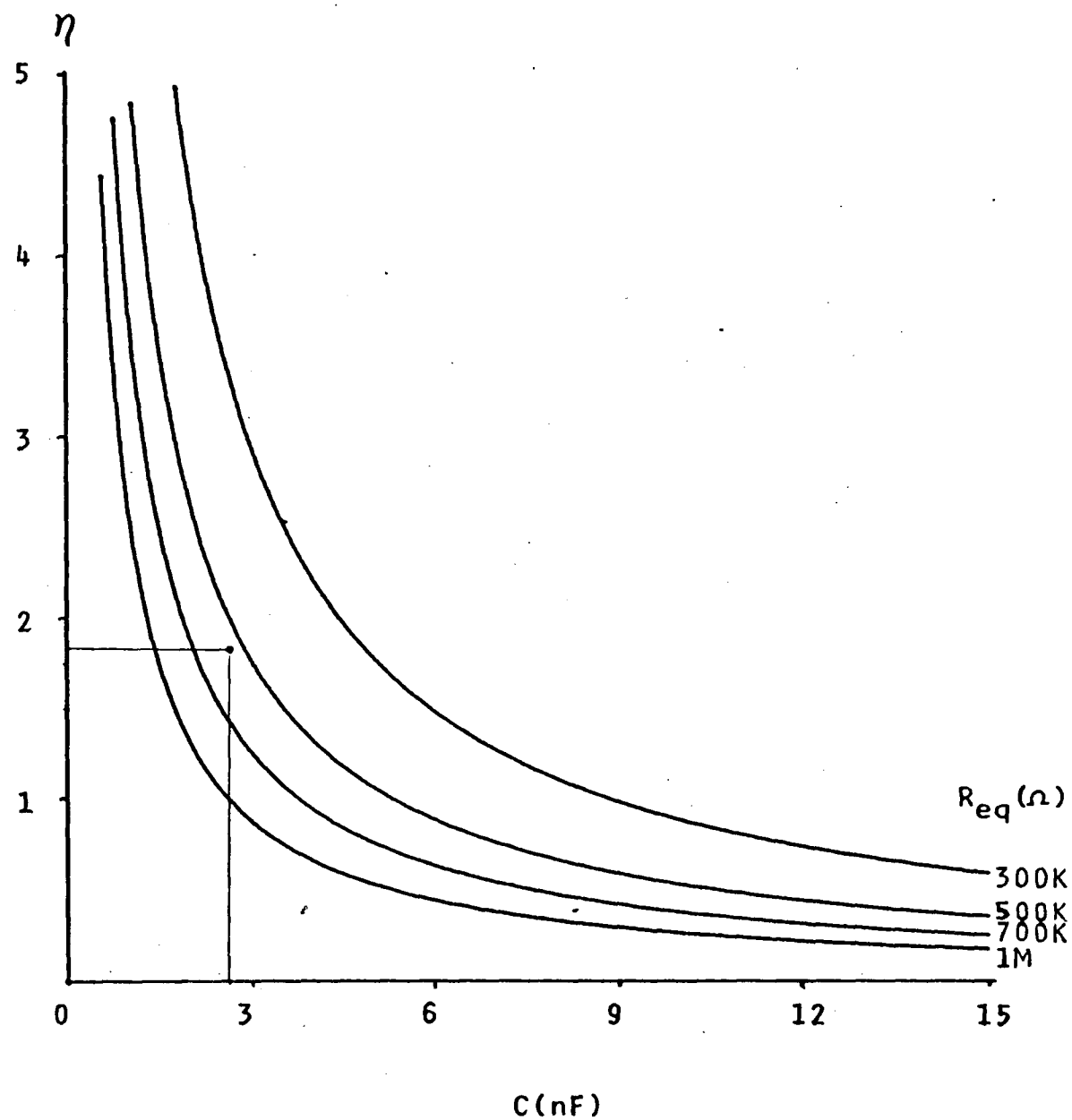

FIGURE 2-22. Circuit Efficiency Design Curves.

Chapter 3 NITROGEN LASER THEORY

3.1 Introduction

The first ultraviolet lasing in nitrogen gas was observed by Heard in 1963 [3]. Using a laser cavity 122 cm in length, Heard observed 30 spectral lines in a 10 W peak power, 20 nsec pulse with the strongest line at 337.1 nm. Since this time, nitrogen laser technique developed rapidly and output powers as high as 2.5 MW in a 4 nsec pulse were soon attainable [4].

The standard physical arrangement of the laser head is shown in Figure 3-1. The nitrogen gas in the cavity is excited by a transverse electron discharge of high current density, 10^4 A/cm^2. [5] During population inversion, the gain is so high, 75 dB/meter [6], that lasing occurs even without the feedback given by mirrors. This effect is often called superradiance though a better name is amplified spontaneous emission. [7] The coherence time is equal to one half the output pulse width[8] and so is only a few nanoseconds. The lateral coherence length is about 5 mm[8] as compared to about 10 cm for He-Ne lasers.

The basic requirements of lasing in nitrogen will be developed in the chapter. The reason why nitrogen lases in a pulsed mode and the effect of increasing the pulse repetition rate is explained. Emphasis will be on the particular needs of a 60 Hz repetition rate.

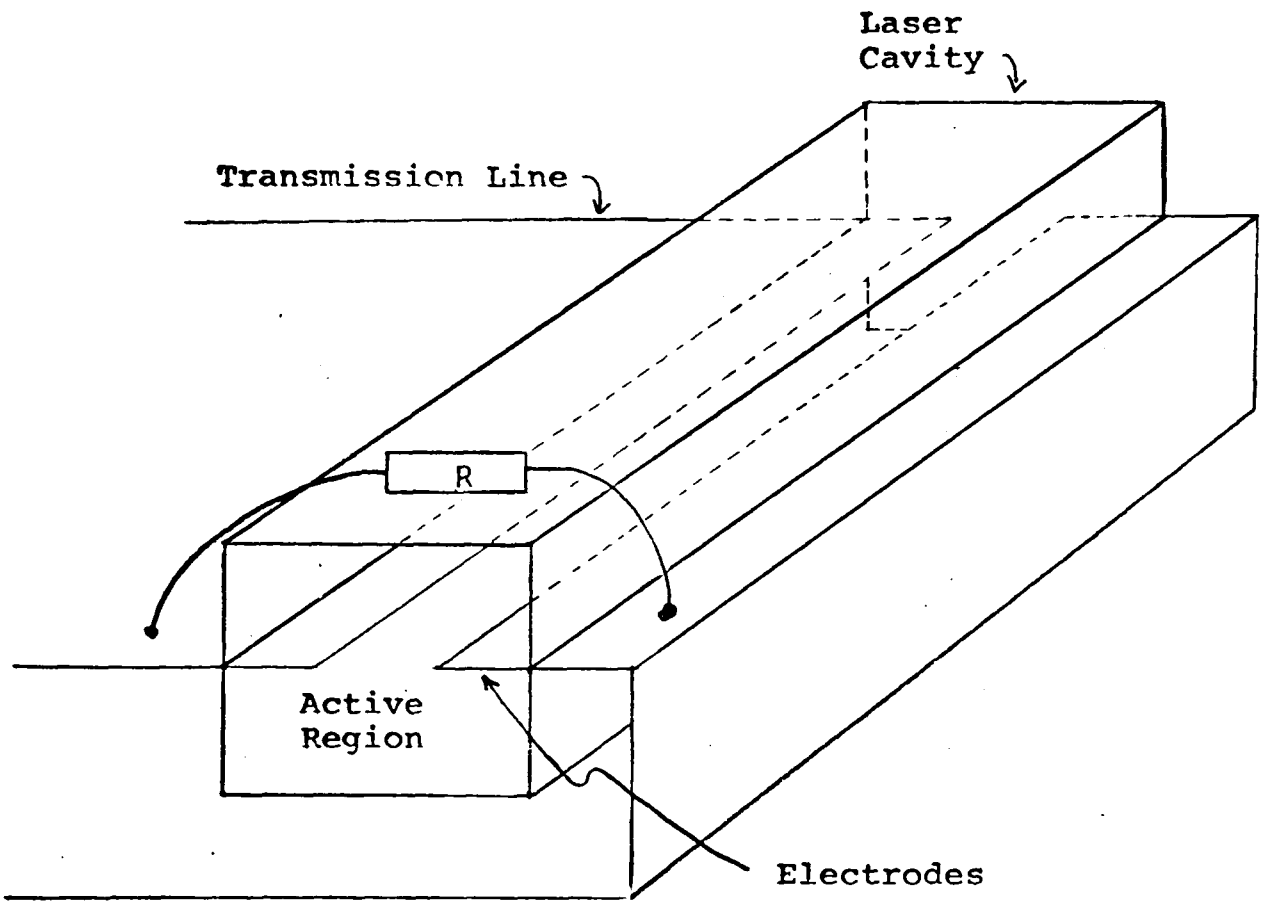

FIGURE 3-1. Laser Head Construction.

3.2 Nitrogen Laser Spectrum

The nitrogen laser output wavelength is actually a group less than .1 nm wide of closely spaced lines centered around 337.1 nm. The qualitative nature of this spectrum will now be described. This discussion is based on the molecular energy levels and the electronic transitions.

Molecular spectra are characterized by three types of transitions; electronic, vibrational and rotational. Electronic transitions are the most energetic, producing photons in the visible and ultraviolet regions. Vibrational transitions with smaller energy differences produce photons in the near infrared; these levels show up as fine structure on the electronic transitions. Rotational transitions are of low energy, giving photons in the far infrared and microwave regions which show up as fine structure on the vibrational spectrum. The N_2 laser is a four-level laser because the lower level is more than a few kT above the ground state as shown in Figure 3-2. Lasing occurs between the $C^3\Pi_u$ upper level and the $B^3\Pi_g$ lower level for the $v=0 \rightarrow 0$ transition of the second positive system of nitrogen where v is the vibrational quantum number. The meaning of the spectroscopic designations $C^3\Pi_u$, etc., is explained in Appendix C. The $B^3\Pi_g$ lower state eventually decays nonradiatively to the ground state $X'\Sigma_g^+$.

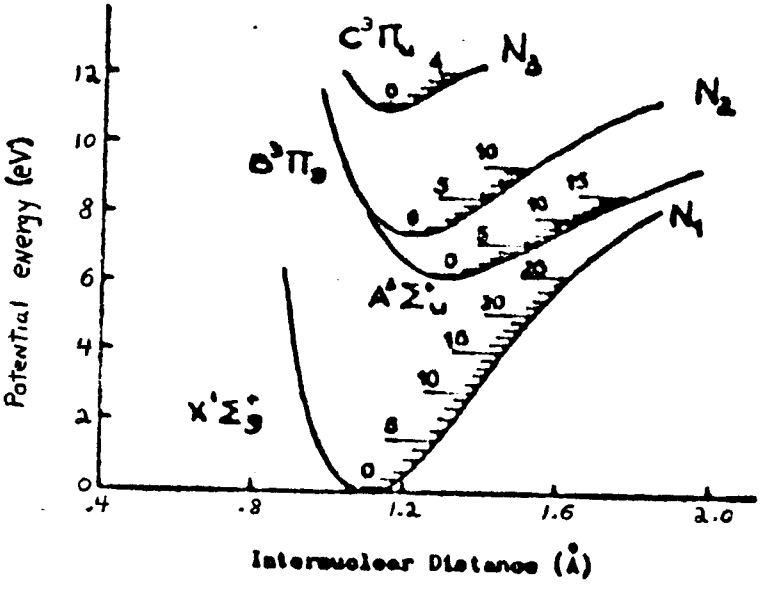

FIGURE 3-2. Molecular Nitrogen Energy Levels.

Some fraction of the electrons decay to intermediate states such as the $A^3\Sigma_u$ state before returning to the ground state. The effects of intermediate states on laser behavior is discussed in Section 3.4.

For the ultraviolet N_2 laser transition, the vibrational quantum number v remains constant so no vibrational transitions are involved. A typical N_2 laser spectrum is shown in Figure 3-3. The four most prominent peaks in the spectrum are at 337.076, 337.082, 337.115, and 337.144 nm. These lines are due to the rotational fine structure, involving P branch transitions where the rotational quantum number, K, decreases with photon emission. Next the rate equations describing the transisitons between levels will be examined.

3.3 Rate Equations

Equations describing the mechanism of electron transitions will now be given. These mechanisms include effects of pumping, stimulated absorptions and spontaneous and stimulated emission. Conditions required for population inversion are given. Approximations which simplify the equations for easy calculations are described and the results compared with experimental evidence from the literature.

Nitrogen lasers are usually pumped by a transverse electronic discharge where the electrons impart energy to the molecules by collision. Rate equations governing this process will now be given.

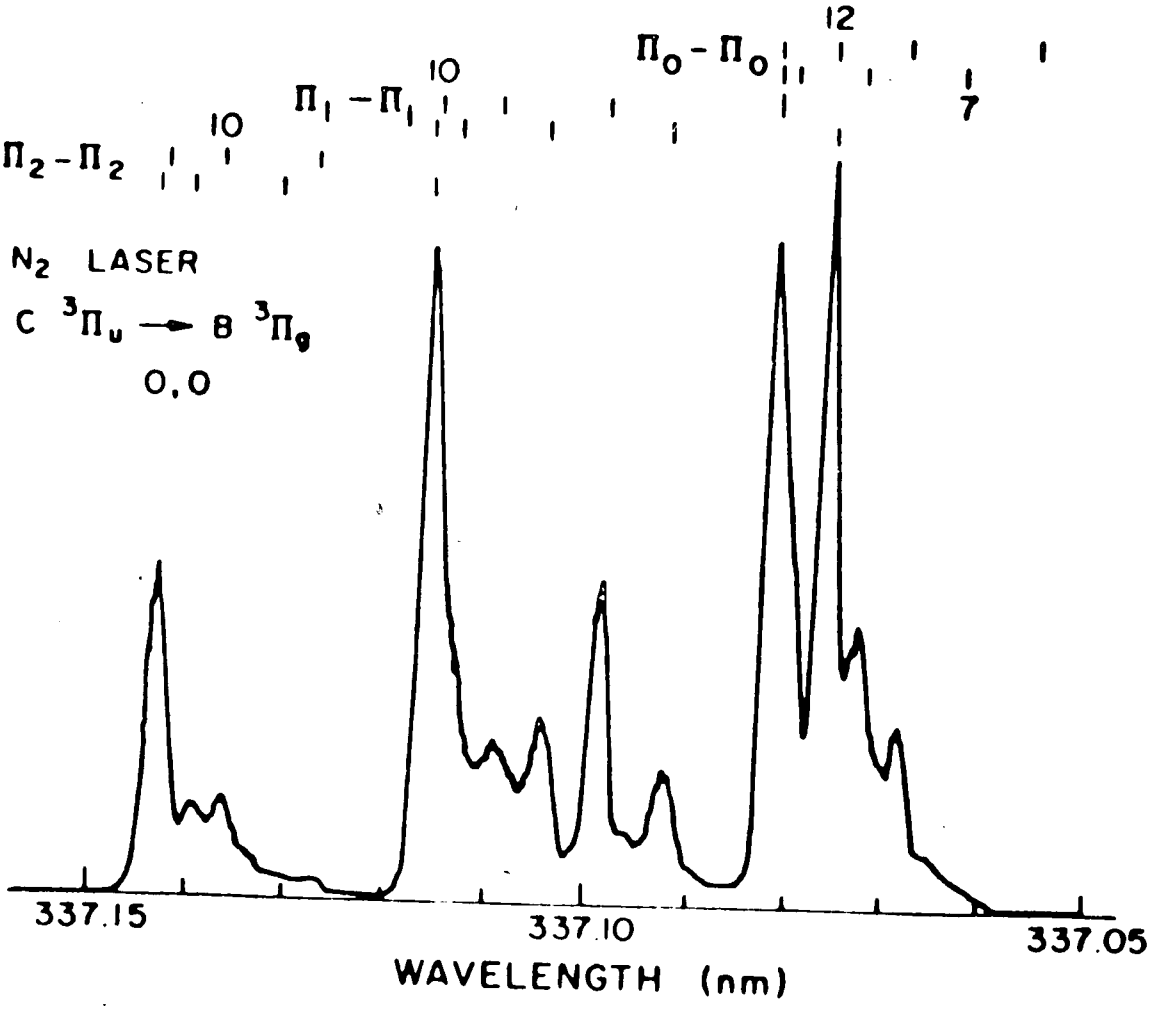

FIGURE 3-3. Nitrogen Laser Spectrum.

Let N_1, N_2, and N_3 denote the populations densities of the ground, lower and upper laser levels.

Then:

$$\frac{dN_3}{dt} = X_{13}N_1 + X_{23}N_2 - (Y_{31} + Y_{32} + \tau_{31}^{-1} + \tau_{32})N_3 - R_{32}[N_3 - (g_3/g_2)N_2] \quad (3-1)$$

$$\frac{dN_2}{dt} = X_{12}N_1 + (\tau_{32}^{-1} + Y_{32})N_3 - (\tau_{21}^{-1} + Y_{21} + X_{23})N_2 + R_{32}[N_3 - (g_3/g_2)N_2] \quad (3-2)$$

$$\frac{dN_1}{dt} = -(X_{12} + X_{13})N_1 + (\tau_{21}^{-1} + Y_{21})N_2 + (\tau_{31} + Y_{31})N_3 \quad . \quad (3-3)$$

The notation is as follows: X_{ij} denotes the electron collisional excitation rate from level i to a higher level j; Y_{ji} denotes the corresponding deexcitation from j to i. Let τ_{ji} be the radiative lifetime of level j before decaying to i and let R_{ji} denote the stimulated transition rate from j to i. Also, g_3 and g_2 are the statistical weights of the upper and lower levels caused by degeneracy of states. These equations are difficult to solve without simplifying assumptions. After Ali et al.,[10] the following assumptions and approximations are made. Because the C state is metastable, or longlived, with respect to the ground state, $\tau_{31} \gg \tau_{32}$. By the Franck-Condon principle which states that electronic collisions preferentially populate levels with the same

internuclear separation as the initial state: $X_{13} > X_{12}$. The spontaneous emission lifetime of the metastable B state is $\tau_{21} \sim 10 \mu sec$; that of the C state is $\tau_{32} \sim 40 nsec$. The simplified equations can be solved to give the results, (using $\tau_{21} \gg \tau_{32}$),

$$N_2 + N_3 = X_{13} N_1 t \qquad (3-4)$$

$$N_2 = \frac{1}{2} X_{13} N_1 (Y_{32} + \tau_{32}^{-1}) t^2 \quad . \qquad (3-5)$$

Combining these equations by eliminating N_1 gives

$$N_3 = \left[\frac{2}{(Y_{32} + \tau_{32}^{-1}) t} - 1 \right] N_2 \quad . \qquad (3-6)$$

For stimulated emission to occur the level populations must be inverted from the equilibrium Boltzmann distribution, so N_3 N_2 requires

$$t < \frac{2}{(Y_{32} + \tau_{32}^{-1})} \quad . \qquad (3-7)$$

This is the inversion condition; it means that for inversion to occur, the excitation time t must obey the inequality. When collisional de-excitation is not important and so $\tau_{32}^{-1} > Y_{32}$, the inequality (3-7) reduces to Bennett's criterion for pulsed laser inversion, given by

$$t < 2\tau_{32} \qquad (3\text{-}8)$$

The domain of validity for these two criteria depends on the electron density of the laser gas. These two inversion criteria will be used in the next section.

Another important simplification is the saturation approximation. For a saturated laser medium, the level inversion, N_3-N_2, is small compared with the total population so

$$N_2 \simeq N_3 \qquad (3\text{-}9)$$

Theoretical output power calculations based on the foregoing simplifications have given excellent agreement with experimental data. This conclusion strongly supports the preceding N_2 laser theory. Laser design requirements based on these results are given next.

3.4 Laser Design Requirements

Results of the experimentally supported theory of the previous sections give important guidelines for laser design. First the energy requirements will be mentioned, followed by the characteristic rise times and recovery times. Finally excitation schemes are briefly discussed.

For collisional excitation, the level of excitation depends on the electron energy. The average electron energy is a gas in proportion to the ratio of external electric field to pressure, E/p. Since different electron energies preferentially populate different energy levels, an optimum E/p can be determined which populates the nitrogen $C^3\Pi_u$ level. The energy level populated by an electron collision is determined by the excitation cross section, σ . A plot of cross section as a function of electron energy for several N_2 levels is given in Figure 3-4. The maximum cross section for the $C^3\Pi_u$ state occurs at 15 ev. The relation of E/p to electron energy is given by

$$E/p = \frac{Energy}{q\lambda p} \qquad (3\text{-}10)$$

where q is the electron charge and λ is the mean free path. Godard has determined λ to be 0.064 cm per torr.[1] Using equation (3-10),

$$E/p = \frac{E_N}{q\lambda p} = \frac{15 \text{ volts}}{.064} = 234 \text{ volts/cm-torr}. \qquad (3\text{-}11)$$

Actually the experimental value is less, being

$$E/p = 200 \text{ volts/cm-torr} \qquad (3\text{-}12)$$

perhaps due to errors in the cross section values.[1] For a given spark gap length, equation (3-12) gives a ratio of optimum voltage to pressure. Bergmann and Eberhardt have shown that a 1 cm laser gap gives the highest output power over a wide range of pressures.[12]

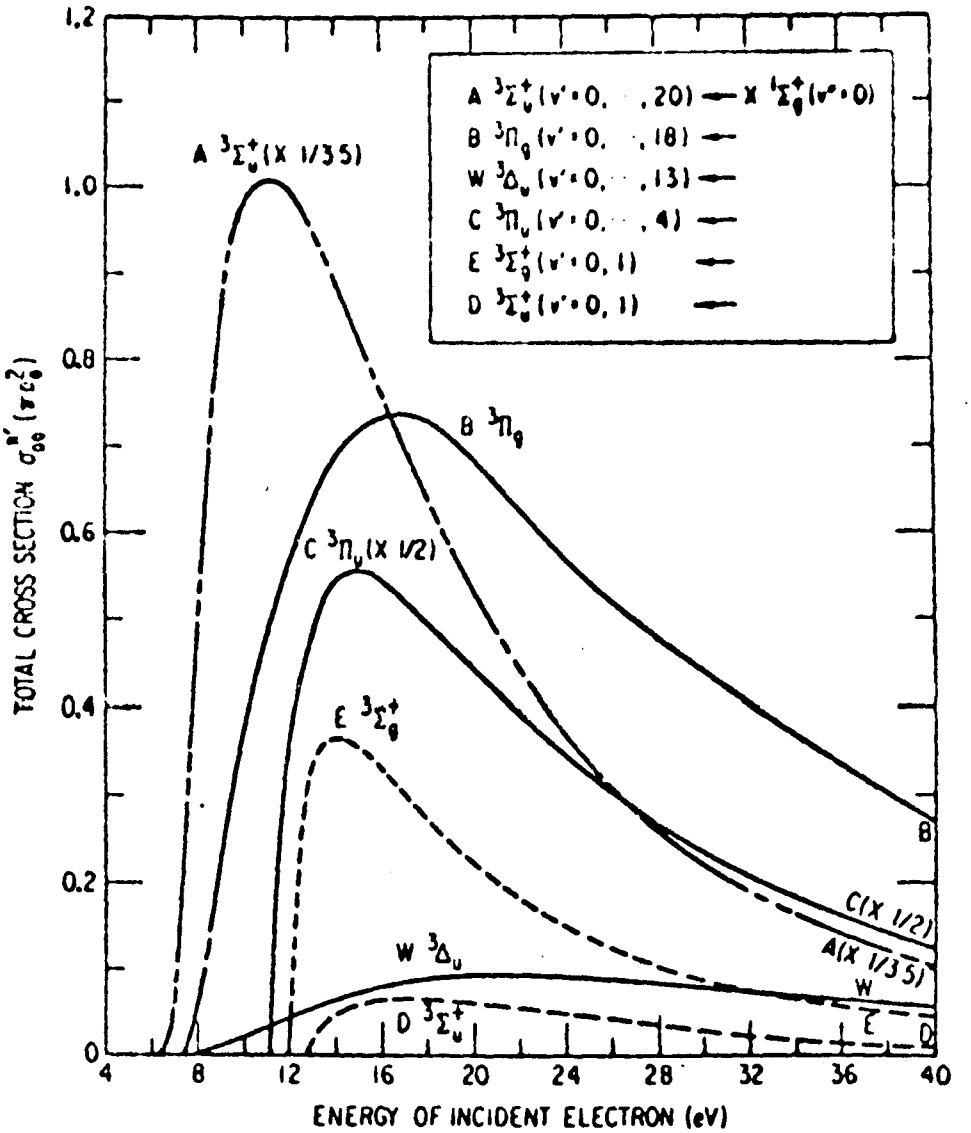

FIGURE 3-4. Nitrogen Electron Excitation Cross Sections.

This optimum choice gives

$$V/p = 200 \text{ volts/torr} \qquad (3\text{-}13)$$

as a design equation for a 1 cm gap.

The level inversion criterion, equation (3-7) gives the maximum permissible excitation time for level inversion. Using values for nitrogen and assuming $Y_{32} << \tau_{32}^{-1}$,

$$t < 2\,\tau_{32} = 80 \text{ nsec}. \qquad (3\text{-}14)$$

However, for pressures greater than 20 torr and with electron densities greater than $6 \times 10^{14} \text{cm}^{-3}$, Y_{32} can be greater than τ_{32}^{-1}.[10] When τ_{32}^{-1} equals Y_{32}, the inversion criterion becomes

$$t < \frac{2}{(Y_{32} + \tau_{32}^{-1})} = 40 \text{ nsec}. \qquad (3\text{-}15)$$

For high pressures the inequality becomes even more restrictive. The conclusion of this analysis is that lasers require excitation pulse times of a few nanoseconds.

The lower laser level, $B^3\Pi_g$, has a long lifetime of 10 μsec and so quickly overpopulates, ceasing level inversion and laser action. Before the laser can be pulsed again the electrons must return to the ground state. Some of the B state electrons nonradiatively decay to intermediate states such as the $A^3\Sigma_u$ state with a radiative lifetime $\tau \sim 1$ sec.[13] These intermediate states preclude repetition

rates of even a few Hertz without the addition of new unexcited gas. For 60 Hz repetition, fresh N_2 gas must flow into the cavity at a high rate.

A large current must pass through the laser gas to yield a large population inversion. For fast excitation, a high voltage transmission line is used to pulse the laser. Results of Chapter 4 show that a shorted transmission line gives a current pulse of amplitude V/Zo where V is the initial voltage and Zo is the line impedance. Therefore high currents require high initial line voltages. The dc breakdown voltage of the laser gas is only about 2000 volts. But a fast rise time pulse can deliver a large over-voltage before the spark gap conducts. Therefore, a voltage pulse having a large dv/dt is needed. This fast voltage pulse is delivered to the pulse line by a spark gap switch which determines the rise time. Now the spark gap breakdown time, during which the voltage changes, is largely independent of the gap over voltage [14], so dv/dt increases with the gap voltage, dt being constant. The conclusion of the foregoing statements is that a large spark gap voltage is needed for a large laser current to give high output power. This conclusion agrees with the experimental evidence of Geller et al. [5]

The V/P requirement of equation (3-13) determines the pressure for highest output power. In practice, V is fixed by the power supply and the pulse line capacitance, so optimum output is

obtained by adjusting the laser pressure.

Chapter 4 SPARK GAP TERMINATED TRANSMISSION LINE

4.1 Introduction

In this chapter some transmission line theory is given along with some gas ionization theory. The goal is to model the nitrogen laser by a high voltage transmission line terminated in a spark gap. This will be done by first analyzing a charged line which discharges into an arbitrary load. Next, gas discharge theory will be used to represent the firing of a laser cavity by a time dependent conductance. The final equations are solved numerically and the results will be examined.

4.2 Transmission Line Theory

A schematic diagram of the nitrogen laser system is shown in Figure 4-1. The laser system comprises two low impedance transmission lines coupled by a spark gap switch. A power supply representing the transformer circuit feeds the energy storage line. The spark gap is approximated by an ideal switch with a small residual inductance, L_s. The pulse forming line delivers energy to the laser channel which is represented as a time dependent conductance, G(t). This circuit will now be investigated using both theoretical calculations and results from the literature.

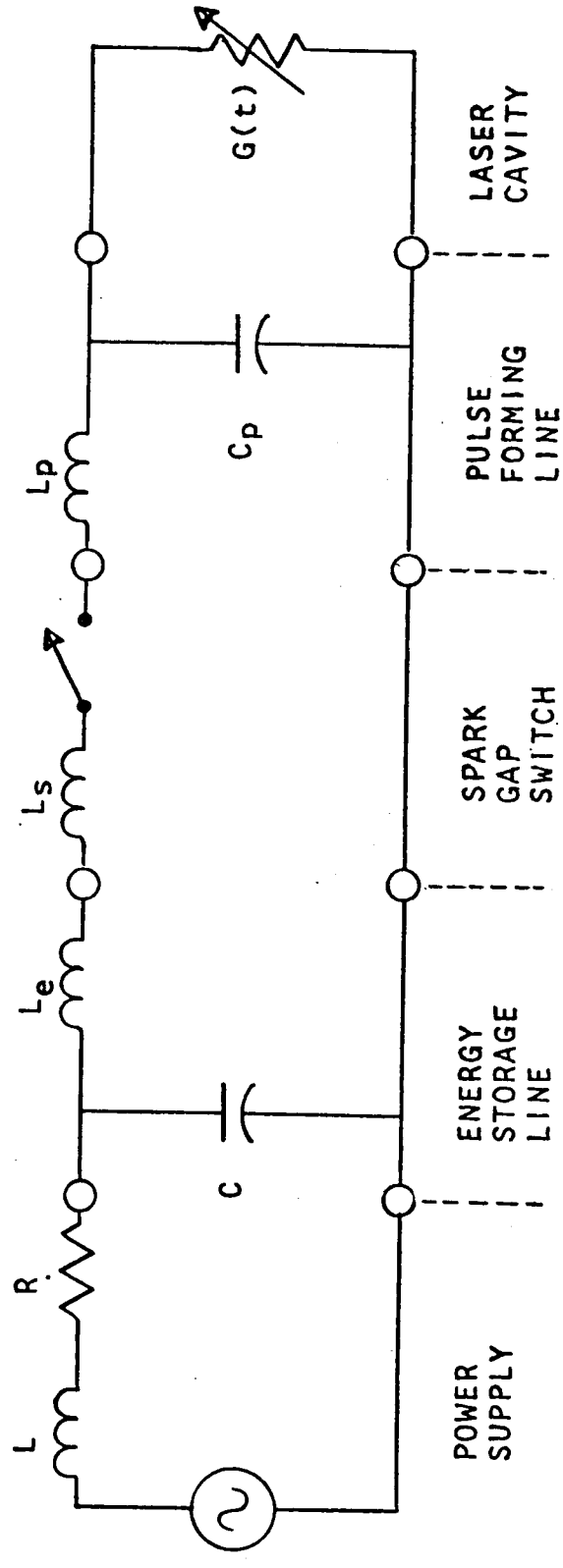

FIGURE 4-1. Schematic of Complete Laser System.

According to Geller et al.[5], the spark inductance, L_s, is large enough so that the pulse line voltage rise follows from lumped circuit analysis. For the circuit of Figure 4-2, Geller gives the pulse line voltage as:

$$V_p(t) = \frac{C}{C + C_p} V_{os}(1 - \cos \omega_r t) \qquad (4\text{-}1)$$

where

$$\omega_r = \left[\frac{C + C_p}{C C_p L_s} \right]^{1/2} \qquad (4\text{-}2)$$

For these equations it was assumed that the initial pulse line voltage and initial current are zero; the initial storage line voltage is V_{os}. The resulting voltage is a sinusoidal oscillation and is lossless because no resistance was assumed. The problem now is to determine the voltages and currents delivered to the laser, making use of equation (4-1) for the pulse line voltage.

Since the pulse times are short, the pulse circuit is represented by distributed parameters. Voltages and currents are d'Alembertian traveling waves with functional dependence given by:

$$V = V(x \pm vt)$$
$$I = I(x \pm vt) \qquad (4\text{-}3)$$

where v is the wave speed and the + sign gives waves traveling in the -x direction and conversely for the - sign. The sign conventions for the wave directions and polarities on a terminated transmission line

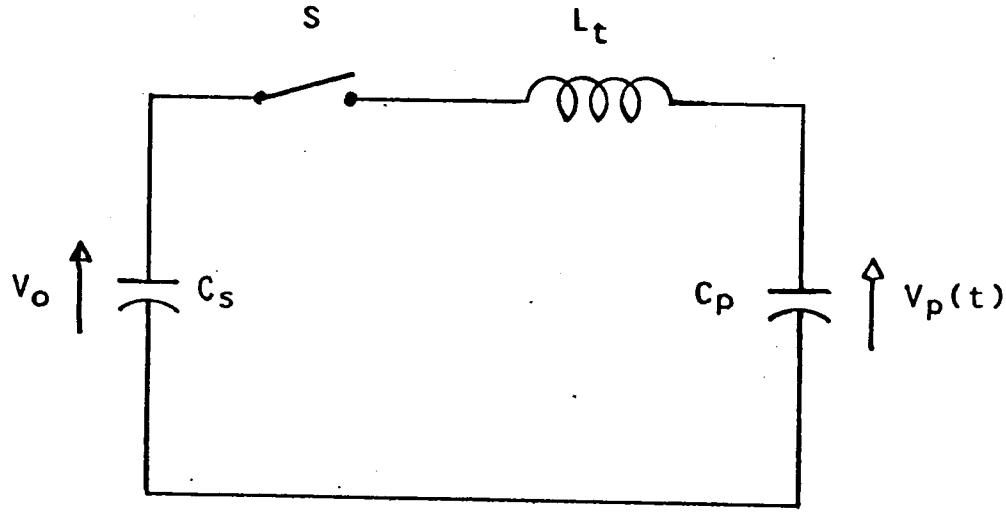

FIGURE 4-2. Pulse Line Lumped Circuit.

are given in Figure 4-3, where 1 denotes a wave to the right and 2 denotes a wave to the left. The traveling voltage and current waves are related by the following equations:

$$I_1 = V_1/Z_o$$

$$I_2 = -V_2/Z_o \qquad (4\text{-}4)$$

where Zo is the characteristic impedance of the line. The total voltage on the line is the initial voltage plus the sum of the traveling waves and likewise for the current.

Consider the terminated pulse line with charging voltage Vp(t), in Figure 4-4. At the point x_2, voltages and currents are related by:

$$I_1 + I_2 = G(t)[V_{op} + V_1 + V_2] \qquad (4\text{-}5)$$

where Vop is the initial pulse line voltage and V_1, V_2 are traveling waves. Both I_1 and V_1 are zero at x_1 because initially no rightward traveling waves exist. Using this fact and the equation (4-4) for V_2:

$$I_2 = G(t)\left[V_{op} - \frac{I_2}{Z_o}\right] \qquad (4\text{-}6)$$

which gives

$$I_2 = \frac{G(t)}{1 + G(t)Z_o} V_{op} \qquad (4\text{-}7)$$

This equation is the desired result, giving the initial laser current drawn from the charged line. The total laser current is I, where

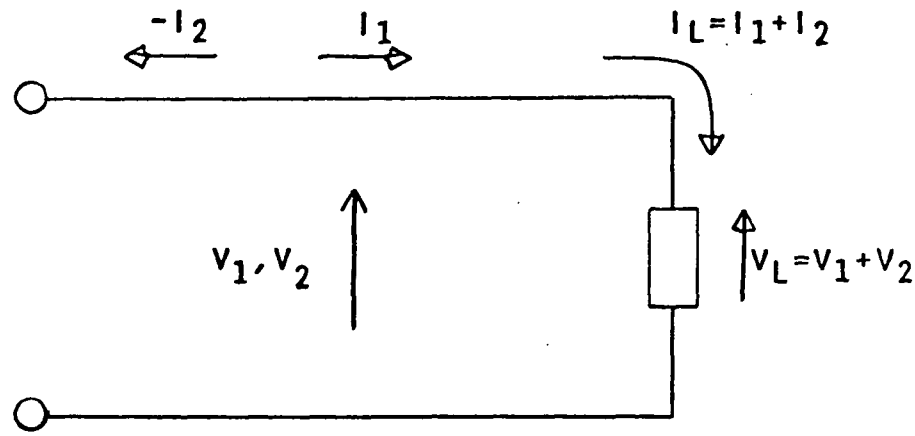

FIGURE 4-3. Transmission Line Sign Conventions.

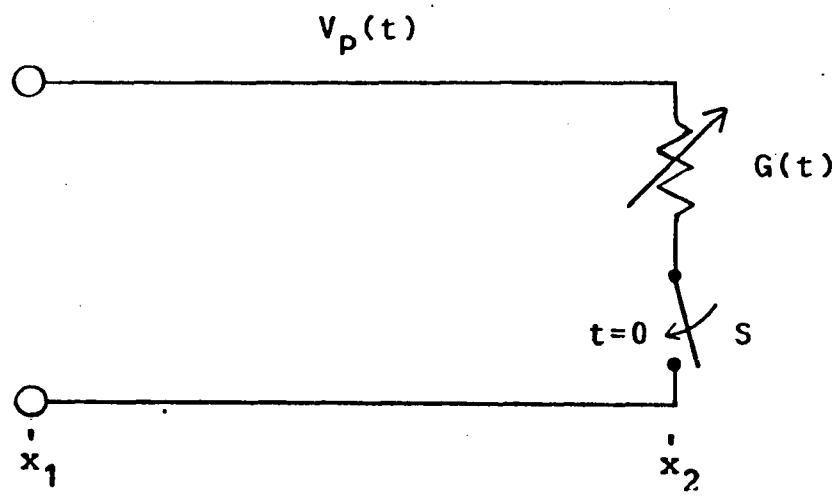

FIGURE 4-4. Terminated Pulse Line.

$$I = I_1 + I_2 \tag{4-8}$$

but initially $I_1 = 0$. Current I_2 travels in the -x direction, reaching x_1, the line end, in a transit time, t_t

$$t_t = \frac{\ell}{v} \tag{4-9}$$

and reflects giving rising to an I_1. This line end is terminated by the spark gap switch and the energy storage line as in Figure 4-1. For the current step reaching x_1, the reactance of L_s is large and so as an approximation, the end can be considered open. The current reflection coefficient [15] of the open end is $\Gamma = -1$ so

$$I_1 = -I_2 \tag{4-10}$$

After an additional transit time, t_t, I_1 reaches the termination and the current flow ceases[23]. Therefore, the total current can be written as

$$I = I_1 + I_2 = I_2(t)\,u(t) - I_2(t - 2t_t)\,u(t - 2t_t) \tag{4-11}$$

where u(t) is the Heaviside unit step function, and $I_2(t)$ given by equation (4-7). Resistance, 1/G(t), becomes vanishing small, $1/G \ll 1\,\Omega$, so good power matching requires a small Z_o. Geller et al. have shown [5] that laser output increases as Z_o is decreased, support-

ing the power matching criterion.

4.3 Gas Ionization Theory

This section presents a derivation of spark gap behavior based on Townsend's gas theory. Some basic spark theory will be presented and a spark gap conductance equation will be derived. This spark equation has not been experimentally verified so the results should be taken hypothetically.

At a given temperature and pressure, a spark gap has a dc breakdown voltage called the spark potential, below which breakdown will not occur. If the voltage is applied suddenly, a time delay called the spark lag, occurs before the spark gap breaks down. This spark lag enables the gap to withstand an overvoltage greater than the spark potential for a short time. Spark lag decreases with the magnitude of overvoltage and with external ionization sources such as ultraviolet light.[16]

Spark gap resistance will now be investigated. Toepler[17] has developed an empirical relation given by

$$R = K \frac{l}{Q(t)} \tag{4-12}$$

where K is the Toepler constant, l is the gap length and Q(t) is the total charge passed through the gap up to time t. This equation accurately gives the final resistance during conduction but is not valid for the initial time development of the spark nor for recombination

effects which stop the spark.[18] Toepler's law and other similar laws are theoretically and experimentally examined by Andreev et al.[14, 19, 20]

A spark law which includes recombination effects can be developed from Townsend's theory.[16] Consider the spark gap in Figure 4-5. The continuity equation for charge carriers is:

$$\frac{\partial n}{\partial t} + \frac{\partial (nv)}{\partial x} = \alpha n v - \beta n \qquad (4\text{-}13)$$

where n is the carrier density, v is the carrier velocity, α is the first Townsend coefficient[21] and β is the carrier recombination rate. The first Townsend coefficient is the number of ion pairs produced by carrier collision in 1 cm of path. Using the expression for current density, J,

$$J = \rho v = q n v \qquad (4\text{-}14)$$

where q is the electronic charge, equation (4-13) becomes

$$\frac{\partial n}{\partial t} + \beta n = \frac{1}{q}\left(\alpha J - \frac{\partial J}{\partial x}\right) . \qquad (4\text{-}15)$$

Since the carriers travel with velocity v, ∂x can be written as

$$\partial x = v \, \partial t \qquad (4\text{-}16)$$

and equation (4-15) becomes

$$\frac{dn}{dt} + \beta n = \frac{1}{q}\left(\alpha J - \frac{1}{v}\frac{dJ}{dt}\right) . \qquad (4\text{-}17)$$

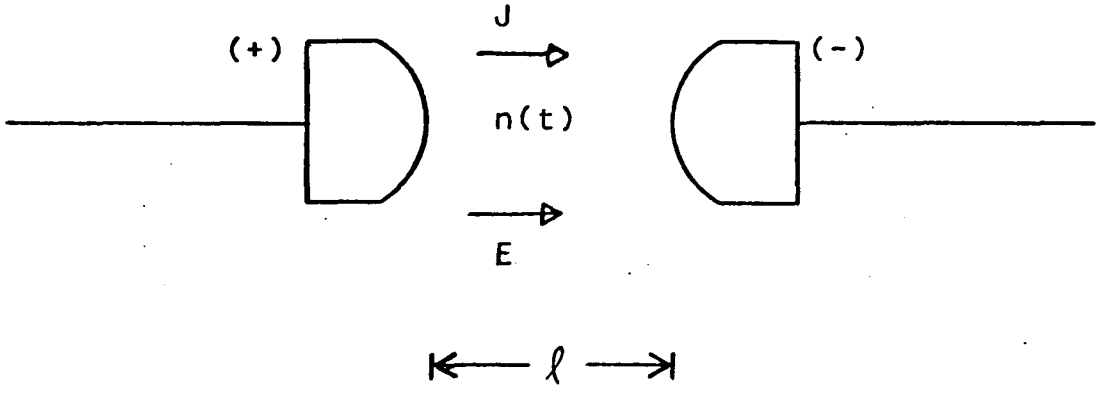

FIGURE 4-5. Spark Gap Current Notation.

The solution of this equation obtained in Appendix D is

$$n(t) = e^{-\beta t} \int_0^t e^{\beta t} \frac{1}{q} \left| \left[\alpha J(t) - \frac{1}{v} \left(\frac{dJ}{dt} \right) \right] \right| dt + n_0 e^{-\beta t} \qquad (4\text{-}18)$$

where n_0 is the initial electron carrier density, and absolute value signs are used because $n(t)$ does not depend on the sign of $J(t)$, only its magnitude. This equation gives the density of electron carriers in the gap as a function of time, and is used to calculate the gap conductance. The definition of conductance is

$$G = \sigma \frac{S}{\ell} \qquad (4\text{-}19)$$

where σ is the conductivity and S is the spark cross-sectional area. The conductivity, σ, depends on n(t) as follows. Ohm's Law in microscopic form is

$$J = \sigma E \qquad (4\text{-}20)$$

Using this and equation (4-14),

$$\sigma = \frac{q\, n(t)\, v}{E} \qquad (4\text{-}21)$$

and by the definition of electron mobility, μ,

$$v = \mu E \qquad (4\text{-}22)$$

equation (4-21) becomes

$$\sigma = q \mu n(t) \; . \qquad (4\text{-}23)$$

Therefore the conductance is

$$G(t) = q\mu \frac{S}{\ell} n(t) \tag{4-24}$$

and substituting for n(t),

$$G(t) = \frac{\mu}{\ell} e^{-\beta t} \left\{ \int_0^t e^{\beta t} \left| \alpha I(t) - \frac{1}{v} \frac{dI}{dt} \right| dt + qS n_0 \right\} \tag{4-25}$$

where I(t) was obtained from J(t) by multiplying by S. Physically, the equation gives the conductance resulting from free electrons in the spark gap gas. The integrand gives the change in electron density due to inflow of current, electron avalanche, and outflow of current. Absolute value brackets are needed because the electron density depends only on the magnitude of current and not its sign. The integration sums over all contributions to electron density throught the time interval and the last term is the initial density. The exponential factor, $e^{-\beta t}$, gives the loss of carriers due to an electron-ion recombination proportional to the total carrier density.

4.4 Composite Equations

The results of the two previous sections will now be combined to give a spark gap terminated line. Equations (4-7) and(4-25) are the relevant formulae. Note that equation (4-25) is an integral

equation; a differential equation can not be obtained because the result depends on the entire past history of the gap. Since the integral kernel, $e^{\beta t}$, is not separable, simple analytical techniques are not applicable.[22] Therefore, a numerical solution, utilizing a computer iteration scheme, will be obtained.

Equation (4-7) can be rewritten in incremental form by taking the differential:

$$dI_2 = \left\{1 - \frac{Z_o}{(1/G(t)) + Z_o}\right\} \frac{V_{op}}{1 + G(t) Z_o} \left[\frac{dG(t)}{dt}\right] dt \quad . \tag{4-26}$$

An expression for dG/dt can be obtained by differentiating G(t) in equation (4-25) and is given by

$$\frac{dG(t)}{dt} = -\beta G(t) + \frac{\mu}{\ell} \left| \alpha I(t) - \frac{1}{v} \frac{dI}{dt} \right| \quad . \tag{4-27}$$

Recall that the total current I(t), given in equation (4-11) is

$$I(t) = I_2(t) u(t) - I_2(t - 2t_t) u(t - 2t_t) \quad . \tag{4-28}$$

This depends only on I_2 so the iteration scheme is

$$I_2(t + dt) = I_2(t) + dI_2 \tag{4-29}$$

where dI_2 is given in equation (4-26), and I(t=o), the initial value, is obtained from equations (4-14) and (4-22) as

$$I(t=0) = S q n_o \mu E = S q n_o \mu \frac{V_{op}}{\ell} \tag{4-30}$$

where $E=V_{op}/\ell$ has been used for the spark gap E field.

4.5 Computer Results

Equation (4-26) was programmed on a CDC 6400 computer to calculate the spark gap current. The initial line voltage, V_{op} in equation (4-26), is given by equation (4-1). This pulse line voltage is slowly varying compared to the traveling wave voltage since:

$$\omega_r = \left[\frac{C + C_p}{C C_p L_s}\right]^{1/2} = 1.2 \cdot 10^8 \text{ rad/sec} \qquad (4\text{-}31)$$

which gives a period T,

$$T = \frac{2\pi}{\omega_r} = \frac{6.28}{1.2} \cdot 10^{-8} = 52 \text{ nsec}. \qquad (4\text{-}32)$$

The current is calculated by an iteration process using finite time intervals and replacing differentials with differences. An initial current value is obtained from equation (4-30) and by using equation (4-26) a new value is caluclated and so on:

$$I(n+1) = I(n) + \Delta I \qquad (4\text{-}33)$$

where n is an integer. A block diagram of the program is given in Figure 4-6 . This program, as the program of Chapter 2, is available on request from Dr. N. Eberhardt at Lehigh University.

One resulting current plot is given in Figure 4-7 . The various physical constants used for this plot are given in Table 4-1.

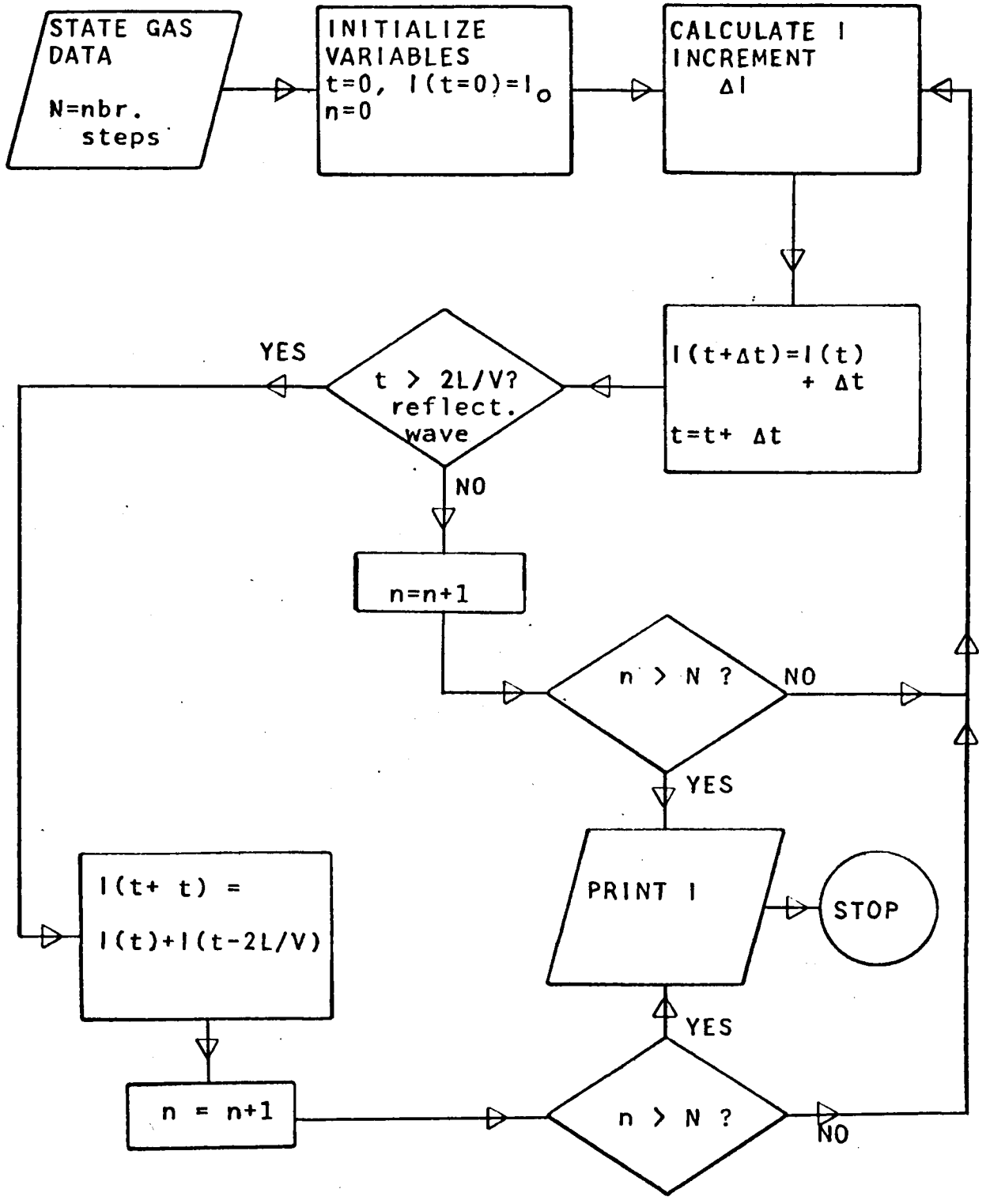

FIGURE 4-6. Block Diagram of Spark Gap Computer Program.

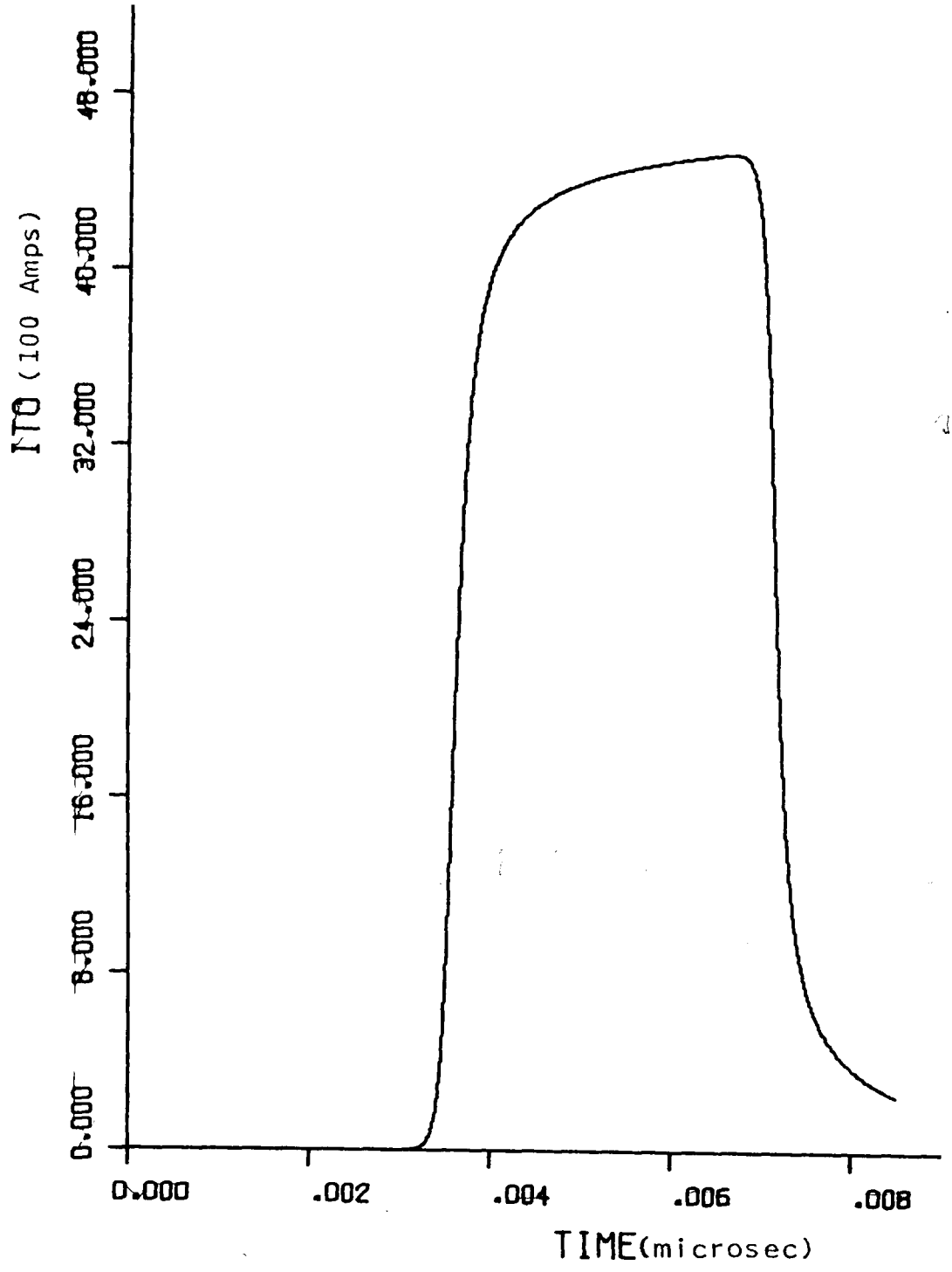

FIGURE 4-7. Spark Gap Current Plot.

TABLE 4-1. Nitrogen Gas Physical Constants.

First Townsend Coefficient/ Pressure Ratio	$\alpha/p_g = 3.0\ cm^{-1}torr^{-1}$
Spark Gap Pressure	$p_g = 100$ torr
Atmospheric Pressure	$p_{atm} = 760$ torr
Carrier Lifetime	$\tau = 10$ nsec
Line Impedance	$Z_o = 1\Omega$
Initial Carrier Density	$n_o = 10^8\ cm^{-3}$
Spark Cross Section	$R_{sp} = 3\times10^{-2}$ cm
Relative Permittivity of Plexiglas Dielectric	$\epsilon_r = 3.12$
Light Speed in Vacuum	$c = 3\times10^{10}$ cm/sec
Electronic Charge	$q = 1.602\times10^{-19}$ coul
Line Loss Resistance	$R = .5$ ohm/meter
Electron Mobility in N_2	$\mu = 2.4\times10^4\ cm^2volt^{-1}sec^{-1}$
Spark Gap Switch Inductance	$L_s = 20$ nH

The calculated pulse compares approximately with the discharge pattern of a charged line suddenly shorted at one end. [23] The pulse edges are rounded due to the dynamic behavior of the spark gap breakdown. The pulse has a duration of twice the line transit time after which time the current flow essentially stops. This current plot is qualitatively comparable to the current measurement of Gerry[11] and also that of Shipman[4] which is shown in Figure 4-8.

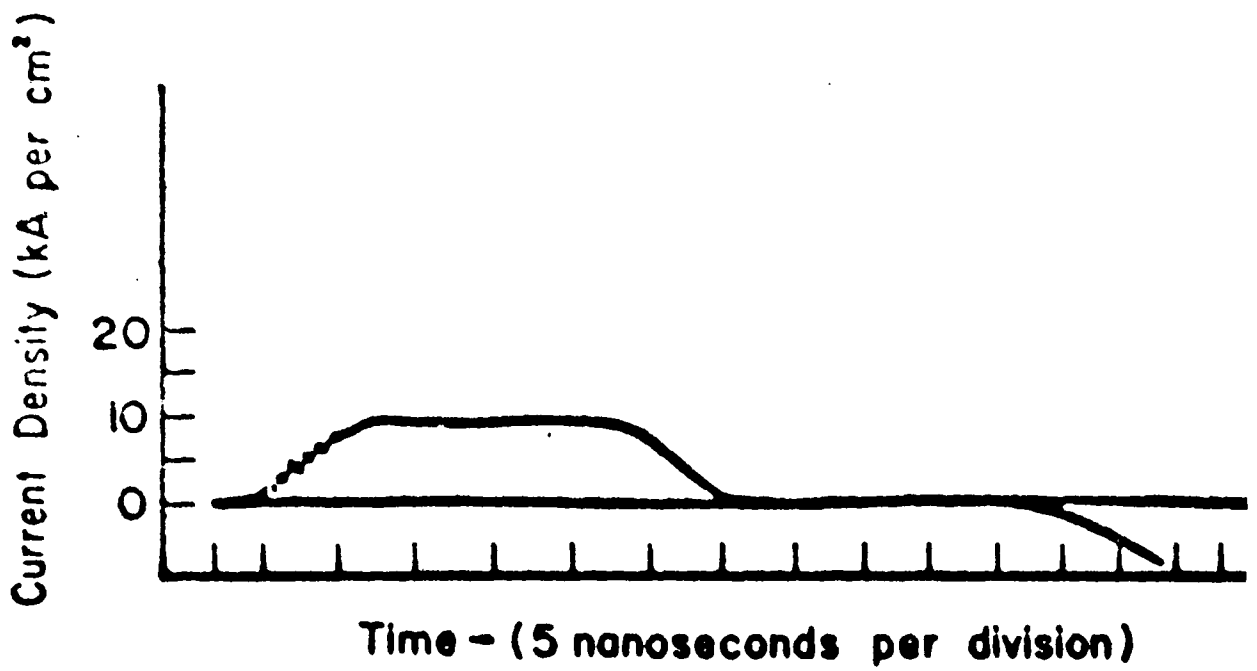

FIGURE 4-8. Spark Gap Current Measurement. (Reference 4).

Chapter 5 LASER CONSTRUCTION AND OPERATION

5.1 Physical Arrangement of Power Supply

A schematic of the power supply circuit is repeated in Figure 5-1 for convenience. A photograph of the actual circuitry is shown in Figure 5-2. The power transformer is fed through a variable transformer for easy voltage adjustment. The 555 K current limiting resistance is supplied by a chain of power resistors. These resistors are connected in series to avoid both resister breakdown and ohmic heating damage. The total power dissipation of the net resistance is

$$P_{diss} = I^2R = (40\,mA)^2 \cdot 555\,K\Omega = 890\ Watts. \tag{5-1}$$

5.2 Transmission Line Arrangement

A drawing of the storage and pulse lines along with the physical dimensions of the conductors is given in Figure 5-3. The actual arrangement is shown in the photograph of Figure 5-4. The conductors were made from .25mm aluminum sheets.

The pulse line dielectric is 2.1mm of plexiglas acrylic, with dielectric constant of 3.12. For a line of 32.5cm, the corresponding two-way transit time is

$$2t_t = \frac{2l\sqrt{\epsilon_r}}{c} = \frac{2 \cdot 32.5 \cdot \sqrt{3.12}}{3 \cdot 10^{10}} = 3.8\ nsec. \tag{5-2}$$

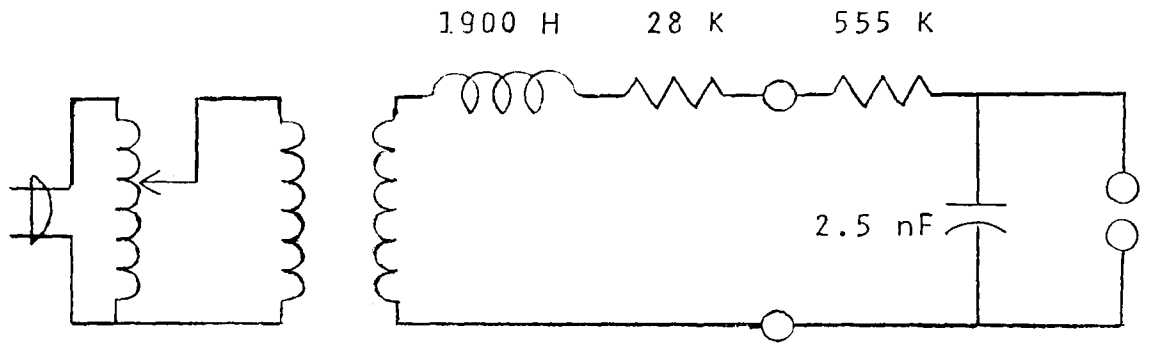

FIGURE 5-1. Power Supply Schematic.

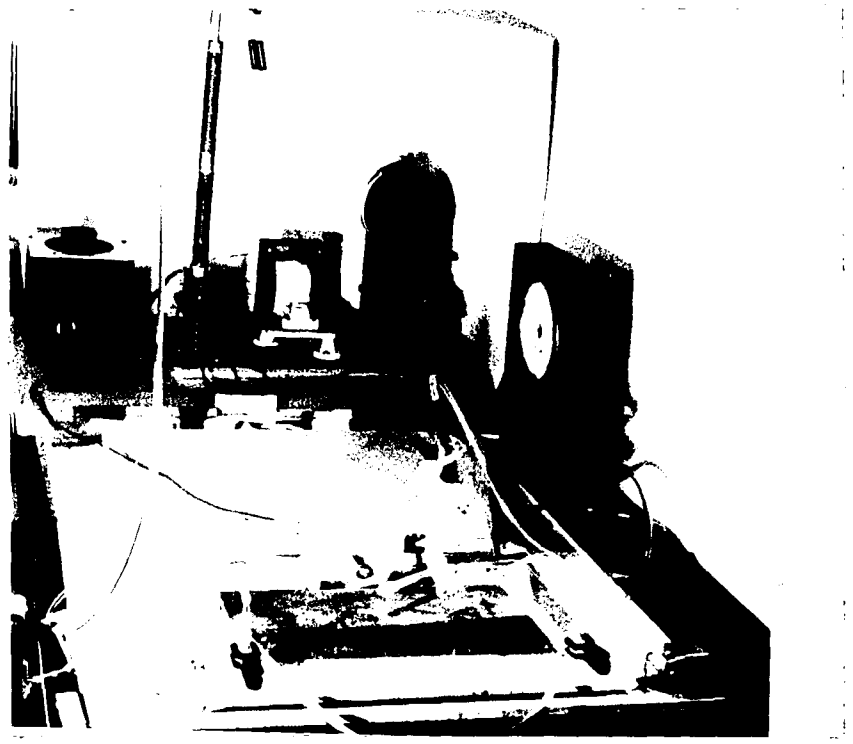

FIGURE 5-2. Power Supply Photograph.

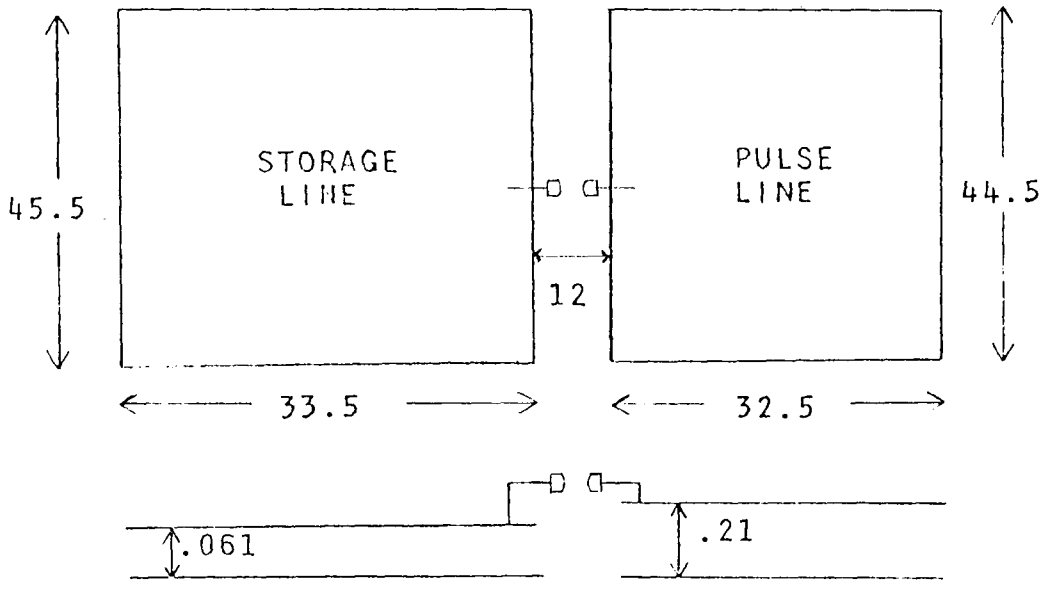

FIGURE 5-3. Transmission Line Construction.
(all measurements in cm)

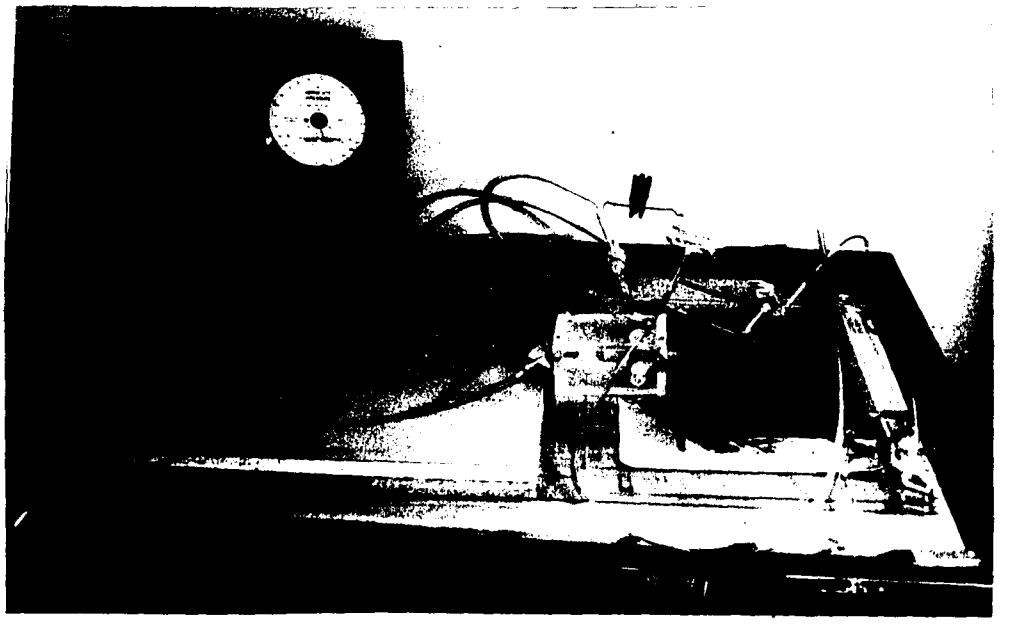

FIGURE 5-4. Transmission Line Photograph.

Total line capacitance as measured by a General Radio type 1650A impedance bridge is .96nF.

The storage line dielectric is 6 sheets of 4 mil (.102mm) Mylar with a dielectric constant of 3.5. With the line length of 35.5 cm the two way transit time is

$$2t_t = \frac{2\ell\sqrt{\epsilon_r}}{c} = \frac{2 \cdot 33.5 \cdot \sqrt{3.5}}{3 \cdot 10^{10}} = 4.2 \text{ nsec} \qquad (5\text{-}3)$$

and total capacitance is 2.71nF. Note that the storage capacitance is larger than the pulse line capacitance (2.71nF vs. .96nF), an arrangement which provides a large pulse line voltage because of the factor, C/(C + Cp), in equation (4-1).

The spark gap switch comprises two brass electrodes mounted in an acrylic box. The electrodes have screw threads so the gap length can be adjusted. Two gas ports are provided and the operating pressure can be varied. The sealed acrylic chamber also helps reduce the noise level of the operating spark gap.

5.3 The Laser Cavity

The laser cavity containing the nitrogen gas was constructed from an acrylic chamber using silicone rubber as cement. This cavity is shown in the photograph of Figure 5-4, and the cross section is drawn in Figure 5-5. The cavity is made of two halves which are glued lengthwise to the conductors.

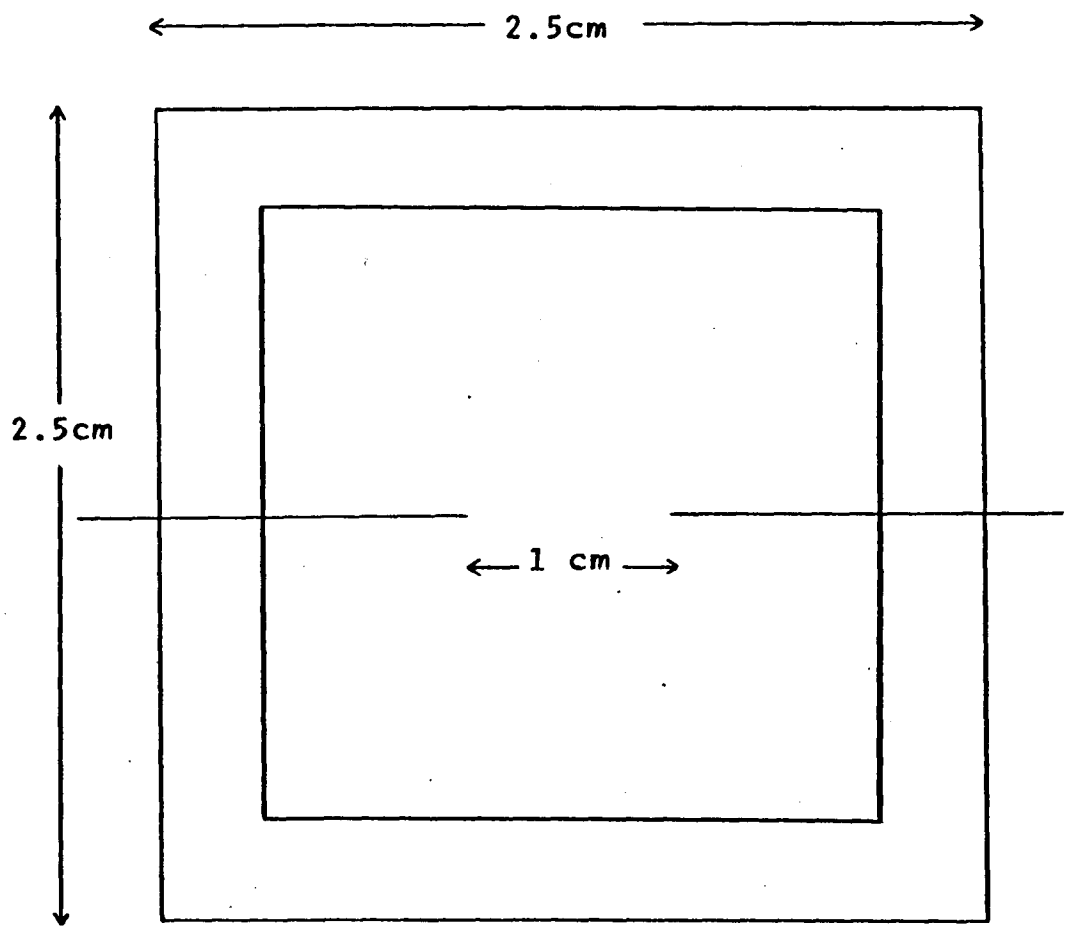

CAVITY LENGTH, L = 51 cm.

FIGURE 5-5. Laser Gap Construction.

Microscope slides are used for end windows and are tilted about 30° to avoid confusing reflections. The entire cavity must be vacuum tight, since operating pressure is only a few torr (mm Hg). Nitrogen gas is admitted through an inlet port and removed from an outlet by a vacuum pump. Cavity pressure is monitored by a metal diaphragm vacuum gauge.

5.4 Laser Operation

The operating procedure for the laser will now be briefly stated. The adjustable spark gap switch is set so that breakdown just occurs at the maximum obtainable storage capacitor voltage. This gap length is 3.5mm. Fresh gas must be vented through the spark gap chamber to ensure spark shut off after each discharge. Otherwise, the ions, being long lived compared to 60 Hz will permit breakdown more than once per half cycle.

The laser cavity pressure for highest output power is 35 torr. The light output is strong enough to excite an organic dye such as Fluoresceine-Na to superradiance when focused by a cylindrical lens. Average power as measured with a Scientech 1-inch disc calorimeter and type 363 power meter is

$$P_{ave} = .65 \text{ mW} \quad . \tag{5-4}$$

The N_2 flow rate through the laser at this power was .03 liter/sec at 1.2 atmospheres of pressure. Smaller flow rates reduced the output power. At 120 Hz operation, the average energy per pulse is

$$E_{ave} = .65\ mW \cdot \frac{1}{120}\ sec = 5.4\ \mu Joule . \qquad (5\text{-}5)$$

An oscillogram of the optical output pulse is given in Figure 5-6. The FWHM (Full Width Half Maximum) pulse length is:

$$\Delta t = 3\ n sec . \qquad (5\text{-}6)$$

This pulse was detected by a Hewlett-Packard 5082-4220 PIN photodiode with a reverse bias of 120 VDC. The laser output was focused on the diode junction for maximum signal. A Tektronix 7904 oscilloscope with a 50 ohm input was used to display the diode signal.

Equations (5-5) and (5-6) can be combined to estimate the peak power:

$$P_{peak} = \frac{E_{PULSE}}{\Delta t} = \frac{5.4\ \mu J}{3 \cdot 10^{-9}\ sec} = 1.8\ KW. \qquad (5\text{-}7)$$

The average output power is comparable to lower repetition rate nitrogen lasers, but the peak power is smaller.

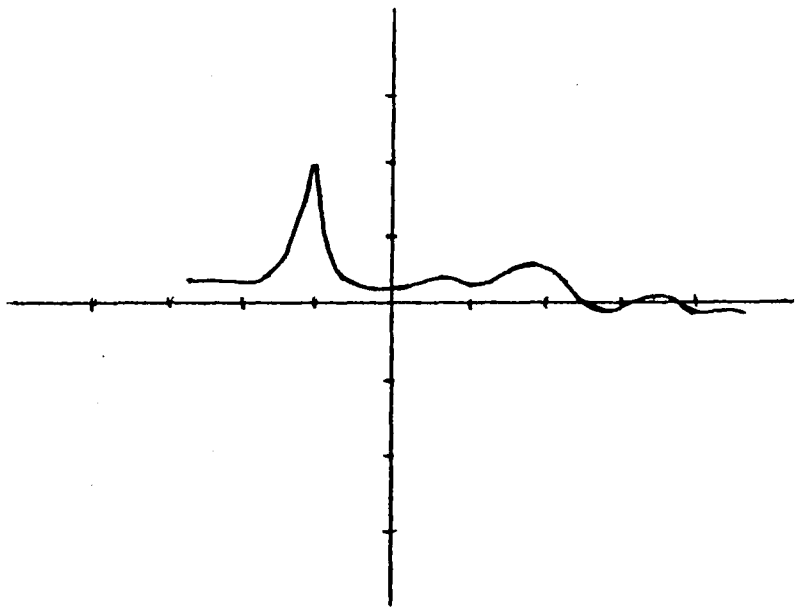

FIGURE 5-6. Laser Output Pulse Photograph.
(Horizontal scale: 5 nsec per division).

Chapter 6 SUMMARY AND SUGGESTION FOR FURTHER STUDY

This thesis has presented an experimental and theoretical investigation of some aspects of a 60 Hz repetion rate N_2 laser. A power supply using a high voltage transformer was constructed. A mathematical circuit model of the power supply was developed and computer plots of the output voltage which agree with experimental results were obtained.

An approximate analysis of the laser was undertaken by modeling the laser as a spark gap terminated transmission line. The results qualitatively agree with experimental findings in the literature.

An attempt was made to keep the thesis approach general. It is hoped that the general guidelines presented here will be useful in the design of other nitrogen lasers. The power supply which employs capacitive discharge circuitry can be used for any pulsed gas laser. For these different gases, the pulse forming line length must be redesigned to accommodate the gas excitation time.

The investigations in this thesis are not exhaustive. Approximations were made and some of the theory has not been experimentally verified. Therefore, many areas mentioned in this thesis can benefit from further study. The author believes that further research on the storage and pulse lines is needed. The analysis of the spark gap

terminated line using gas theory could be extended to include the non-ideal spark gap switch which connects the storage line to the pulse line. As yet, it is not quite certain whether the discharge of the storage line can be described by lumped circuit analysis. The dynamic behavior of the discharge circuit should be studied with a high voltage oscilloscope.

Bibliography

1. B. Godard, "A Simple High-Power Large-Efficiency N_2 Ultraviolet Laser", IEEE J. Quantum Electron., vol. QE-10, pp. 147-153, Feb. 1974.

2. L. W. Matsch, "Electromagnetic and Electromechanical Machines," Scranton: Intext Educational Publishers, 1972.

3. H. G. Heard, "Ultraviolet Gas Laser at Room Temperature", Nature, 200, 667, Nov. 1963.

4. J. D. Shipman, "Traveling Wave Excitation of High Power Gas Lasers", Appl. Phys. Lett., vol. 10, pp. 3-4, Jan 1967.

5. M. Geller, D. E. Altman, and T. A. DeTemple, "Some Considerations in the Design of a High Power, Pulsed N_2 Laser", Appl. Opt. vol. 7, pp. 2232-2237, Nov. 1968.

6. D. A. Leonard, "Saturation of the Molecular Nitrogen Second Positive Laser Transition", Appl. Phys. Lett., vol. 7, pp. 4-8, Jul. 1965.

7. L. Allen and G. I. Peters, "Amplified Spontaneous Emission and External Signal Amplification in an Inverted Medium", Phys. Rev. A, vol. 8, pp. 2031-2047, Oct. 1973.

8. O. Steinvall and A. Anvari, "The Design and Coherence Properties of a Simple N_2 Laser", Physica Scripta, vol 3, pp. 1125-1128, Jul 1973.

9. V. M. Kaslin and C. G. Petrash, "Rotational Structure of Ultraviolet Generation of Molecular Nitrogen", JETP Lett., vol. 3, pp. 55-57, Jan. 1966.

10. A. W. Ali, A. C. Kolb, and A. D. Anderson, "Theory of the Pulsed Molecular Nitrogen Laser", Appl. Opt., vol. 6, pp. 2115-2119, Dec. 1967.

11. E. T. Gerry, "Pulsed Molecular Nitrogen Laser Theory", Appl. Phys. Lett., vol. 7, pp. 6-8, Jul. 1965.

12. E. E. Bergmann and N. Eberhardt, "A Short High Power TE Nitrogen Laser", IEEE J. Quantum Electron. (Corresp.), vol. QE-9, pp.853-854, Aug. 1973.

13. B. W. Woodward, V. J. Ehlers, and W. C. Lineberger, "A Reliable, Repetitivly Pulsed, High-Power Nitrogen Laser", Rev. Sci. Instrum., vol. 44, July 1973.

14. S. I. Andreev and M. P. Vanyukov, "Application of a Spark Discharge to Obtain Intense Light Flashes of Length 10^{-7}-10^{-8} Sec.", Sov. Phys.-Tech. Phys., vol. 6, pp.700-708, Feb. 1962.

15. R. E. Collin, "Field Theory of Guided Waves", New York: McGraw-Hill, 1960.

16. J. J. Thomson and G. P. Thomson, "Conduction of Electricity Through Gases". New York: Dover, 1955.

17. M. Toepler, Archiv fur Electrotechnik, XVIII Band, pp 549-566, 1927.

18. F. Frungel, "High Speed Pulse Technology", vol.II. New York: Academic Press, 1965.

19. S. I. Andreev and B. I. Orlov, "Development of a Spark Discharge I", Sov. Phys.-Tech. Phys., vol.10, pp.1097-1101, Feb. 1966.

20. S. I. Andreev and B. M. Sokolov, "Breakdown Mechanism of a Narrow Air Gap. II", Sov. Phys.-Tech. Phys., vol. II, pp.254-256, Aug. 1966.

21. J. S. Townsend, "Electricity in Gases". London: Oxford University Press, 1915.

22. G. Arfken, "Mathematical Methods for Physicists". New York" Academic Press, 1970.

23. J. Millman and H. Taub, "Pulse, Digital, and Switching Waveforms". New York: McGraw-Hill, 1965.

APPENDIX A

Transformer Measurements

The transformer to be measured is a Thordarson type 2470 iron core power transformer. Primary voltage is 110 VAC and the secondary voltage is 25 KVAC. The corresponding turns ratio is a, where

$$a = \frac{N_1}{N_2} = 4.4 \cdot 10^{-3} = \frac{1}{226} \qquad \text{(A-1)}$$

The power handling limit is 1000 VA. The transformer equivalent circuit will now be measured.

Starting with the exact transformer equivalent circuit of Figure A-1, the primary and secondary winding resistances R_1 and R_2 are measured.[2] The results are

$$R_1 = 0.20\,\Omega$$
$$R_2 = 18.0\,\Omega \quad . \qquad \text{(A-2)}$$

The remainder of the measurements are based on the approximate equivalent circuit of Figure A-2 which is valid for iron core transformers. To measure r_1 and l_1, the secondary is opened up and the primary is driven by a voltage source as in Figure A-3. Now I_{exc} is measured by A, V_{oc} is measured by V and the power dissipated in r_1 is measured by W. These measurements must be corrected for instrument losses as follows

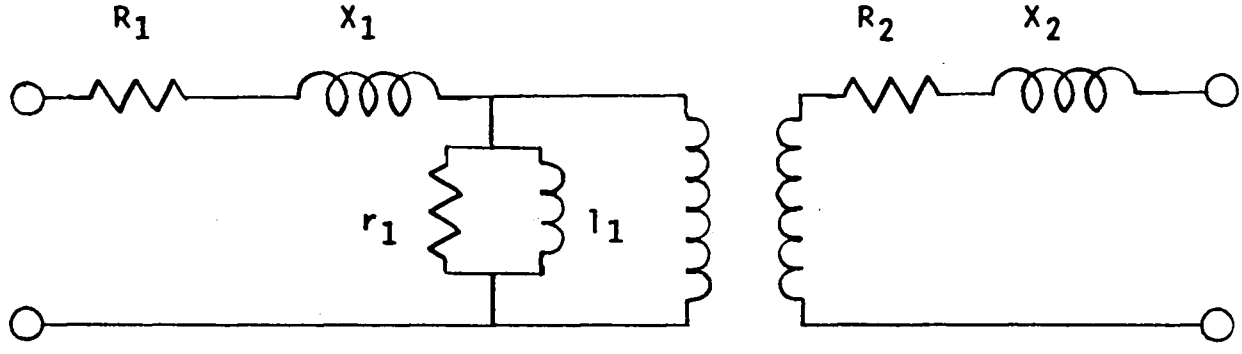

FIGURE A-1. Transformer Equivalent Circuit.

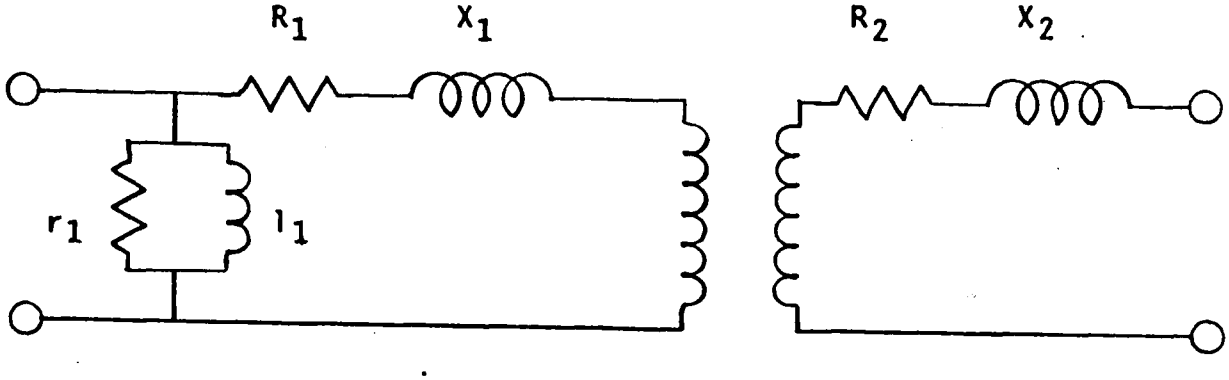

FIGURE A-2. Approximate Equivalent Circuit.

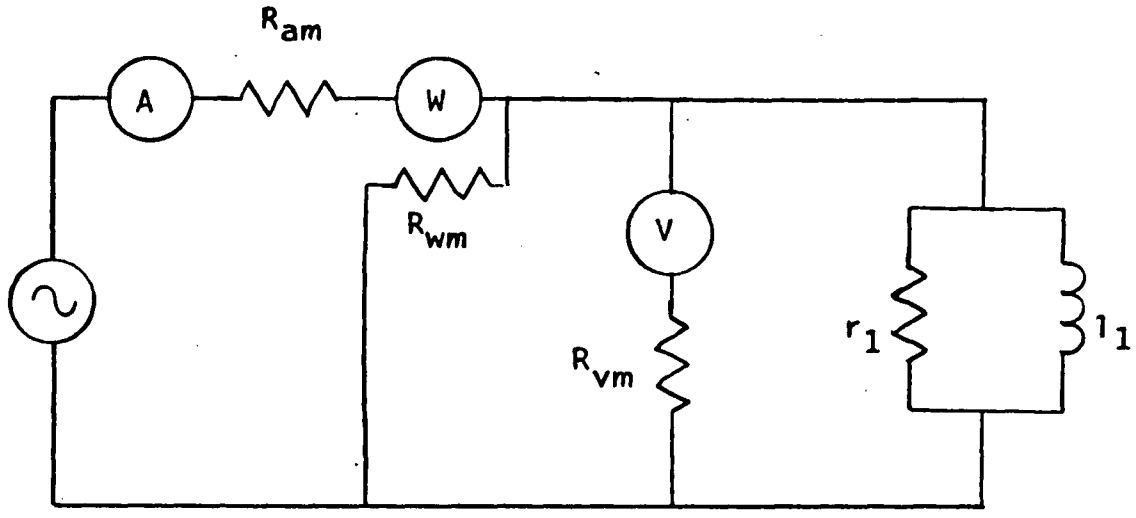

FIGURE A-3. Transformer Measurement Circuit.

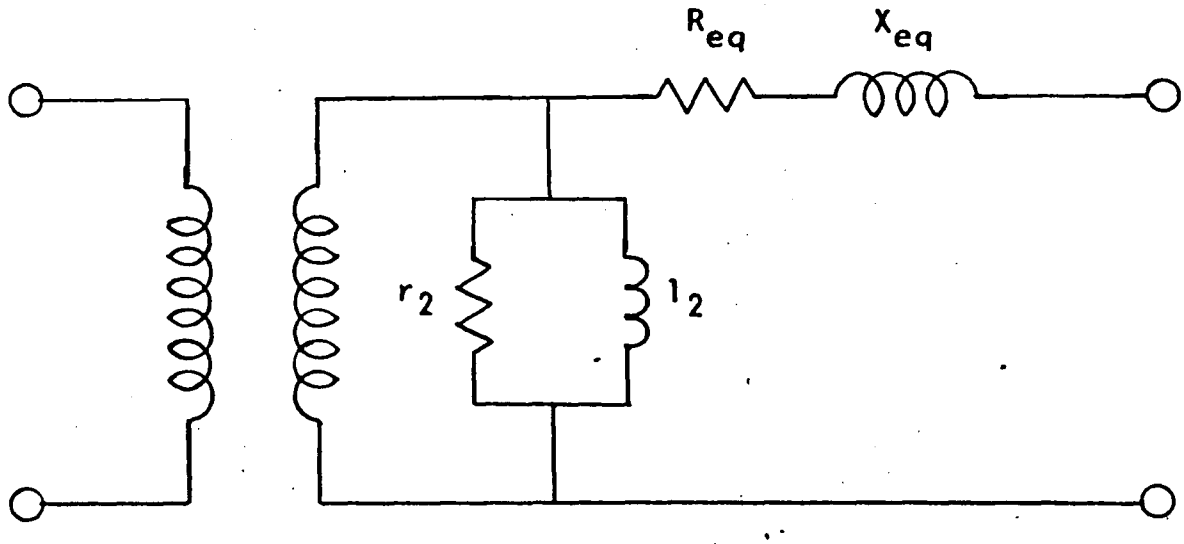

FIGURE A-4. Transformer Secondary Measurements.

$$V_{oc} = V = 100.\ v \tag{A-3}$$

$$P_{oc} = W - \frac{V^2}{R_{VM}} - I^2 R_{AM} = 69.8\ W$$

$$I_{exc} = A - \frac{V}{R_{WM}} - \frac{V}{R_{VM}} = 3.89\ A\ .$$

These numbers give

$$|y| = \frac{I_{exc}}{V_{oc}} = 38.9\ mmhos$$

$$g_1 = \frac{P_{oc}}{V_{oc}^2} = 6.98\ mmhos \tag{A-4}$$

$$b_1 = \sqrt{|y|^2 - g_1^2} = 38.2\ mmhos$$

or

$$r_1 = 145\ \Omega$$

$$l_1 = 69\ mH\ .$$

Referring the circuit to the secondary as in Figure A-4 it follows:

$$R_{eq} = \frac{R_1}{a^2} + R_2 = 28.3\ K\Omega \tag{A-5}$$

$$r_2 = \frac{r_1}{a^2} = 7.48\ M\Omega$$

$$l_2 = \frac{l_1}{a^2} = 3560\ H\ .$$

X_{eq} is measured by shorting the primary, thereby shorting r_1, l_1, and taking voltage and current measurements as in Figure A-5. From the measurements of V and I, it follows

$$X_{eq} = \sqrt{\left(\frac{V}{I}\right)^2 - R_{eq}^2} \qquad (A\text{-}6)$$

$$L_{eq} = \frac{X_{eq}}{\omega} \quad .$$

The result is

$$L_{eq} = 1900\ H\ . \qquad (A\text{-}7)$$

A summary of the measurements is given in Figure A-6.

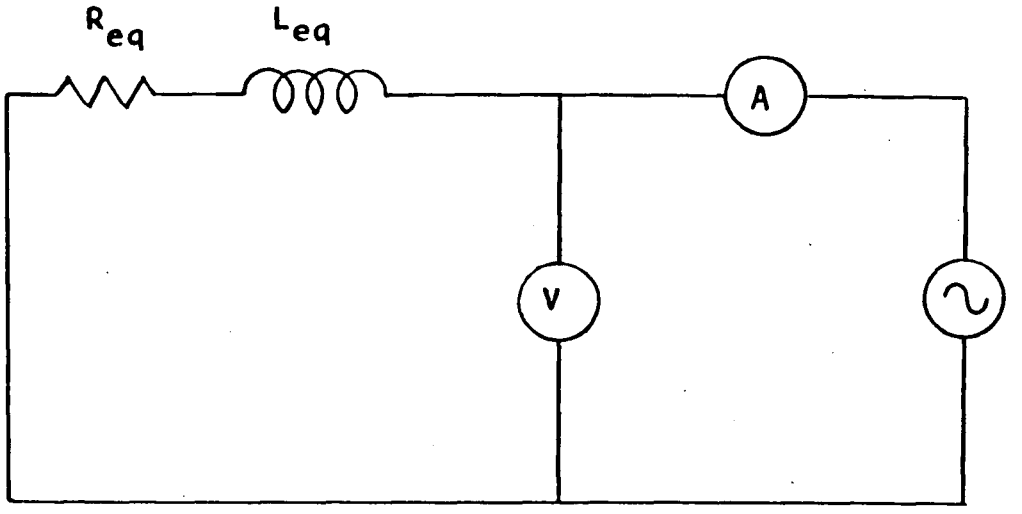

FIGURE A-5. Measurement of R_{eq}, L_{eq}.

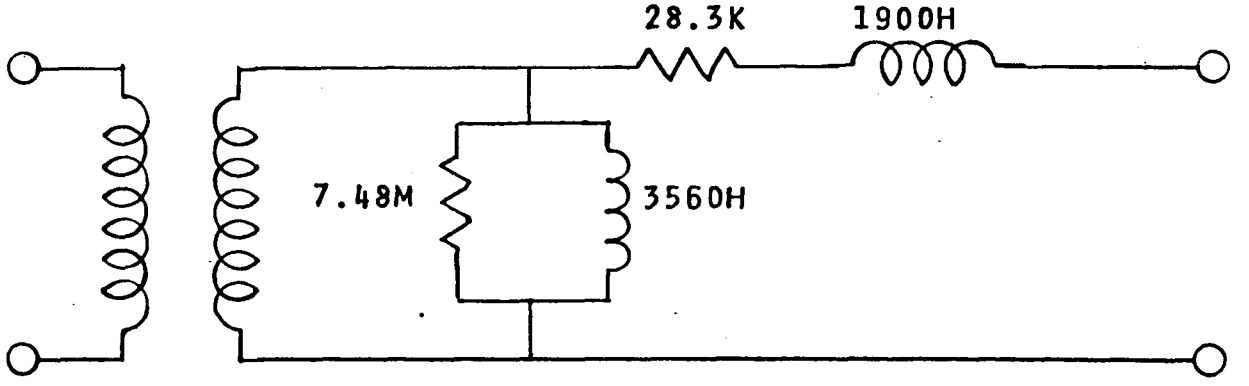

FIGURE A-6. Summary of Measurements.

APPENDIX B

Capacitor Waveforms

The capacitor voltage and current response to a sinusoidal driving voltage and with arbitrary initial conditions will now be calculated. The initial conditions are the capacitor voltage, series current and source phase. The circuit is a series RLC circuit shown in Figure B-1. The capacitor voltage, Vc(t), will be calculated first, including both transient and steady state components. Having the voltage, the current can be easily calculated from the relation:

$$i_c(t) = C \frac{dv_c(t)}{dt} \qquad \text{(B-1)}$$

The waveform responses will be underdamped due to the large value of inductance. This is easily proved by showing that the natural frequency is real:

$$\omega_d^2 = \omega_o^2 - \alpha^2 = \frac{1}{LC} - \left(\frac{R}{2L}\right)^2 = 1.7 \cdot 10^6 \gg 0 \qquad \text{(B-2)}$$

thereby showing the response to be underdamped. Because the circuit is linear, the voltage response can be calculated in two steps:

total response = source response with zero initial conditions + zero source response with given initial conditions

The complete source response will be calculated first and then the complete initial condition response.

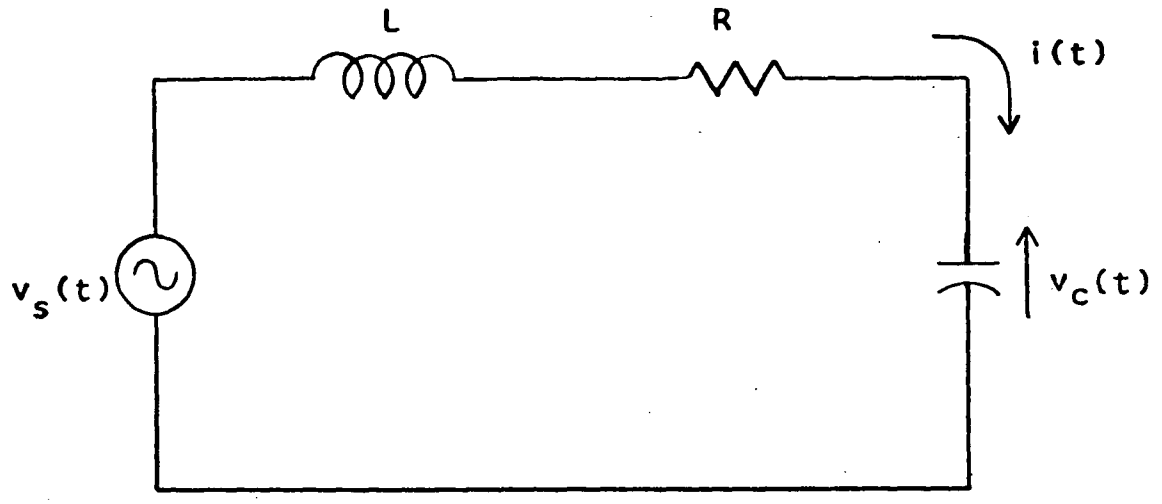

FIGURE B-1. Capacitor Charging Circuit.

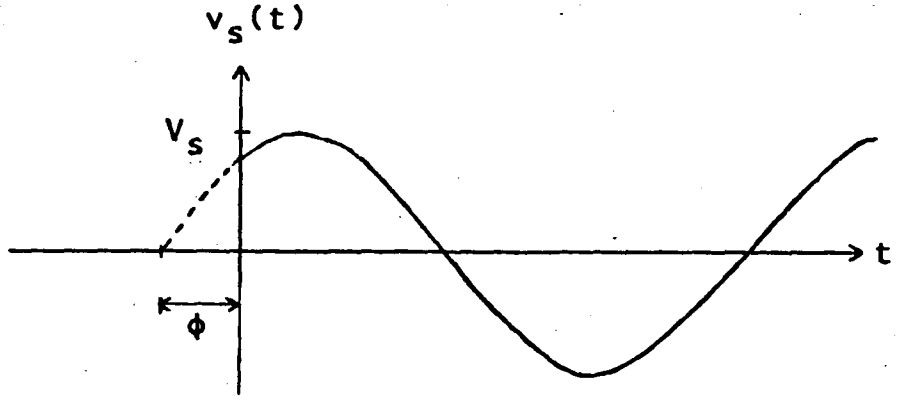

FIGURE B-2. Voltage Source Waveform.

The source voltage will be taken as

$$v_s(t) = V_s \sin(\omega t + \phi)\, u(t) \tag{B-3}$$

where ϕ is the initial phase and u(t) is the Heaviside unit step function. The source term is partially plotted in Figure B-2. To simplify calculations, the source waveform is rewritten as

$$v_s(t) = V_s [\cos\phi \sin\omega t + \sin\phi \cos\omega t]\, u(t) . \tag{B-4}$$

The most straightforward technique for calculating the capitor voltage uses the Laplace transform. Standard tables can be used for determining the transforms and their inverses. Henceforth, the Laplace transform will be designated by $\mathcal{L}$ and its inverse by $\mathcal{L}^{-1}$. The capacitor voltage is determined by

$$v_c(t) = \mathcal{L}^{-1}[V_c(s)] = \mathcal{L}^{-1}[V_s(s)\, H(s)] \tag{B-5}$$

where $V_s(s) = \mathcal{L}[v_s(t)]$ and $H(s)$ is the transfer function defined by

$$H(s) = \frac{\mathcal{L}[v_c(t)]}{\mathcal{L}[v_s(t)]} . \tag{B-6}$$

H(s) can be determined directly from the circuit using Kirchhoff's laws. The Laplace transform of the source term is now obtained.

Using Equation (B-4) and proceeding:

$$V_s(s) = \mathcal{L}[v_s(t)]$$

$$= \frac{V_s \cos\phi \; \omega}{(s+j\omega)(s-j\omega)} + \frac{V_s \sin\phi \; s}{(s+j\omega)(s-j\omega)} \quad . \tag{B-7}$$

Next the transfer function is obtained using complex voltage division:

$$H(s) = \frac{V_c(s)}{V_s(s)} = \frac{1/sC}{1/sC + sL + R} = \frac{1/LC}{s^2 + \frac{R}{L}s + \frac{1}{LC}} \tag{B-8}$$

For simplicity, the following definitions are made:

$$\omega_o = \frac{1}{\sqrt{LC}}$$

$$\alpha = \frac{R}{2L} \tag{B-9}$$

$$\omega_d = \sqrt{\omega_o^2 - \alpha^2}$$

The source frequency is w and is 377 rad/sec for 60 Hz. The roots of the denominator of H(s) in equation (B-8) are

$$s_{1,2} = -\frac{R}{2L} \pm j\sqrt{\frac{1}{LC} - \left(\frac{R}{2L}\right)^2} \tag{B-10}$$

$$= -\alpha \pm j\omega_d \quad .$$

Forming the product for the capacitor voltage:

$$V_c(s) = V_s(s)\,H(s) = \frac{V_s \cos\phi \; \omega \omega_o^2}{(s^2+\omega^2)(s-s_1)(s-s_2)} + \frac{V_s \sin\phi \; s \; \omega_o^2}{(s^2+\omega^2)(s-s_1)(s-s_2)} \tag{B-11}$$

Taking the inverse transform:

$$v_c(t) = \mathcal{L}^{-1}[V_c(s)] = \omega\omega_o^2 V_s \cos\phi \left\{ \frac{e^{s_1 t}}{(-s_2+s_1)(s_1^2+\omega^2)} \right.$$

(B-12)

$$\left. + \frac{e^{s_2 t}}{(-s_1+s_2)(s_2^2+\omega^2)} + \frac{SIN(\omega t - \psi_1)}{\omega\sqrt{\omega^2(-s_1-s_2)^2+(s_1 s_2-\omega^2)^2}} \right\}$$

$$+\omega_o^2 V_s SIN\phi \left\{ \frac{s_1 e^{s_1 t}}{(-s_2+s_1)(s_1^2+\omega^2)} + \frac{s_2 e^{s_2 t}}{(-s_1+s_2)(s_2^2+\omega^2)} \right.$$

$$\left. + \frac{SIN(\omega t + \psi_2)}{\sqrt{(s_1^2+\omega^2)(s_2^2+\omega^2)}} \right\}$$

where,

$$\psi_1 = tan^{-1}\left(\frac{\omega}{s_1}\right) + tan^{-1}\left(\frac{\omega}{-s_2}\right)$$

(B-13)

and

$$\psi_2 = tan^{-1}\left(\frac{-s_2}{\omega}\right) - tan^{-1}\left(\frac{\omega}{-s_1}\right)$$

(B-14)

Further simplifying and substituting for s_1, s_2,

$$v_c(t) = \omega_o^2 V_s \frac{e^{-\alpha t}}{\omega_d}\left[\frac{(\alpha^2-\omega_d^2+\omega^2)\sin\omega_d t + 2\alpha\omega_d\cos\omega_d t}{(\alpha^2-\omega_d^2+\omega^2)^2 + 4\alpha^2\omega_d^2}\right]$$

$$\times(\omega\cos\phi - \alpha\sin\phi)$$

$$+ \omega_o^2 V_s \sin\phi\, e^{-\alpha t}\left[\frac{(\alpha^2-\omega_d^2+\omega^2)\cos\omega_d t - 2\alpha\omega_d\sin\omega_d t}{(\alpha^2-\omega_d^2+\omega^2)^2 + 4\alpha^2\omega_d^2}\right]$$

$$+ \frac{\omega_o^2 V_s\cos\phi\sin(\omega t - \psi_1)}{\left[(\omega_o^2-\omega^2)^2 + 4\alpha^2\omega^2\right]^{1/2}}$$

$$+ \frac{\omega_o^2 V_s\sin\phi\sin(\omega t + \psi_2)}{\left[(\alpha^2-\omega_d^2+\omega^2)^2 + 4\alpha^2\omega_d^2\right]^{1/2}} \qquad \text{(B-15)}$$

where

$$\psi_1 = \tan^{-1}\left\{\frac{2\alpha\omega}{\omega_o^2-\omega^2}\right\} \quad ; \quad \psi_2 = \tan^{-1}\left\{\frac{\omega_o^2-\omega^2}{2\alpha\omega}\right\} \qquad \text{(B-16)}$$

This is the underdamped capacitor voltage due to source response only.

The response due to arbitrary initial conditions will now be calculated. The circuit of interest is given in Figure B-3. The differential equation governing the capacitor voltage is

$$\frac{d^2 v_c(t)}{dt^2} + 2\alpha\frac{dv_c}{dt} + \omega_o^2 v_c = 0 \qquad \text{(B-17)}$$

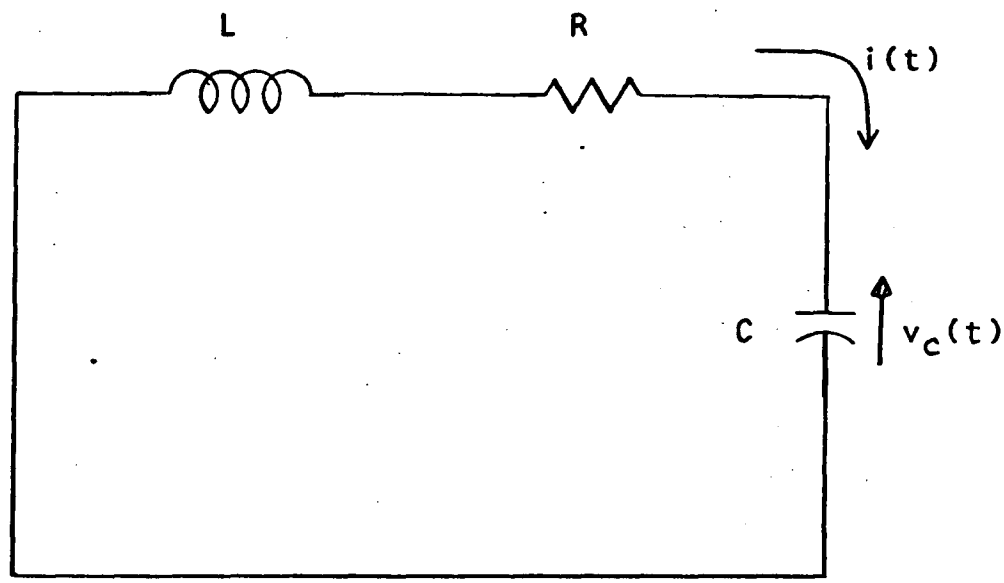

FIGURE B-3. Initial Condition Circuit.

The initial conditions are Vc(o) equals Vco and $i(0) = I_o$.

The solution of this equation for the underdamped response is standard and is given in many texts on circuit theory:

$$v_c(t) = V_{co}\frac{\omega_o}{\omega_d}e^{-\alpha t}\cos(\omega_d t-\theta) + \frac{I_o}{\omega_d C}e^{-\alpha t}\sin\omega_d t$$

where $\theta = \tan^{-1}\left(\frac{\alpha}{\omega_d}\right)$. (B-18)

The complete response to both source and initial conditions is the sum of equations (B-15) and (B-18),

$$v_c(t) = \omega_o^2 V_s e^{-\alpha t}\left\{\left[\frac{(\alpha^2-\omega_d^2+\omega^2)\sin\omega_d t + 2\alpha\omega_d\cos\omega_d t}{(\alpha^2-\omega_d^2+\omega^2)^2 + 4\alpha^2\omega_d^2}\right]\right.$$

$$\left.\times\left(\frac{\omega}{\omega_d}\cos\phi - \frac{\alpha}{\omega_d}\sin\phi\right)\right.$$

$$+\sin\phi\left[\frac{(\alpha^2-\omega_d^2+\omega^2)\cos\omega_d t - 2\alpha\omega_d\sin\omega_d t}{(\alpha^2-\omega_d^2+\omega^2)^2 + 4\alpha^2\omega_d^2}\right]$$

$$+\frac{\omega_o^2 V_s\cos\phi\sin(\omega t-\psi_1)}{\left[(\omega_o^2-\omega^2)^2+4\alpha^2\omega^2\right]^{1/2}} + \frac{\omega_o^2 V_s\sin\phi\sin(\omega t+\psi_2)}{\left[(\alpha^2-\omega_d^2+\omega^2)^2+4\alpha^2\omega_d^2\right]^{1/2}}$$

$$+ V_{co}\frac{\omega_o}{\omega_d}e^{-\alpha t}\cos(\omega_d t-\theta) + \frac{I_o}{\omega_d C}e^{-\alpha t}\sin\omega_d t$$

(B-19)

where

$$\psi_1 = \tan^{-1}\left\{\frac{2\alpha\omega}{\omega_o^2-\omega^2}\right\} \quad ; \quad \psi_2 = \tan^{-1}\left\{\frac{\omega_o^2-\omega^2}{2\alpha\omega}\right\} \qquad \text{(B-20)}$$

$$\theta = \tan^{-1}\left\{\frac{\alpha}{\omega_d}\right\}$$

The series current follows from Equation (B-1) and is:

$$i_c(t) = \omega_o^2 C V_s e^{-\alpha t}\left\{\left[\frac{\left(\frac{\omega}{\omega_d}\right)\cos\phi - \left(\frac{\alpha}{\omega_d}\right)\sin\phi}{(\alpha^2-\omega_d^2+\omega^2)^2+4\alpha^2\omega_d^2}\right]\right. \qquad \text{(B-21)}$$

$$\times\left[\omega_d(\omega^2-\alpha^2-\omega_d^2)\cos\omega_d t - \alpha(\alpha^2+\omega_d^2+\omega^2)\sin\omega_d t\right]$$

$$-\frac{\sin\phi}{(\alpha^2-\omega_d^2+\omega^2)^2+4\alpha^2\omega_d^2}\left[\alpha(\alpha^2+\omega_d^2+\omega^2)\cos\omega_d t\right.$$

$$\left.\left.+\omega_d(\omega^2-\alpha^2-\omega_d^2)\sin\omega_d t\right]\right\}$$

$$+\frac{\omega\omega_o^2 C V_s\cos\phi\cos(\omega t-\psi_1)}{\left[(\omega_o^2-\omega^2)^2+4\alpha^2\omega^2\right]^{1/2}} + \frac{\omega\omega_o^2 C V_s\sin\phi\cos(\omega t+\psi_2)}{\left[(\alpha^2-\omega_d^2+\omega^2)^2+4\alpha^2\omega_d^2\right]^{1/2}}$$

$$-\omega_o C V_{co} e^{-\alpha t}\left[\frac{\alpha}{\omega_d}\cos(\omega_d t-\theta) + \sin(\omega_d t-\theta)\right]$$

$$+I_o e^{-\alpha t}\left[\cos\omega_d t - \frac{\alpha}{\omega_d}\sin\omega_d t\right] \quad .$$

APPENDIX C

Molecular Spectroscopic Classification

The notation convention for diatomic molecular energy levels will now be given. The molecular angular momentum vector along the internuclear axis, z, given by $\vec{\Omega}$, has two components; orbital angular momentum, $\vec{\Lambda}$, and spin angular momentum, $\vec{\Sigma}$. The vector $\vec{\Sigma}$ is the z component of total spin $\vec{S}$. Since the vectors $\vec{\Omega}$, $\vec{\Lambda}$, $\vec{\Sigma}$ lie along z, they can be added algebraically.

$$\Omega = |\Lambda + \Sigma| \tag{C-1}$$

Where the absolute value is taken because the quantum number Ω is positive only. Orbital momentum Λ can take on only integral values with $\Lambda = 0, 1, 2, 3, ..$ designated by $\Sigma, \Pi, \Delta, \Phi, ...$ respectively, analogous to the atomic S, P, D, F levels. The z component, Σ of S can take on the values:

$$\Sigma = -S, -(S-1), \ldots, 0, \ldots, S-1, S \tag{C-2}$$

The multiplicity of states is given by:

$$2S + 1 \tag{C-3}$$

because the electronic state splits into 2S+1 levels due to magnetic interaction with the orbital momentum, Λ . By convention, 2S + 1 is called the multiplicity even if there is no splitting as when $\Lambda = 0$.

The diatomic molecule has two types of symmetry. The first type concerns electron wave function reflection through any plane

which lies along the z axis. If the electron wave function does not change sign by reflection, it is a + state, if it changes sign it is a - state. The other type of symmetry is by reflection through the plane which perpendiculary bisects the z axis. If the wave function does not change sign, it is even, designated by g (gerade); if it changes sign it is odd designated by u (ungerade).

The standard molecular classification type is given by

$$^{(2S+1)}\Lambda^{a}_{b} \qquad \text{(C-4)}$$

where Λ takes on values $\Sigma, \Pi, \Delta,$ etc., "a" can be plus or minus, and "b" either g or u. Sometimes different levels can be designated by the same classification so that a prefix given by A, B, .. z, a, b... is added to avoid confusion. As examples, consider the nitrogen laser levels $C^3\Pi_u$ and $B^3\Pi_g$; these are both triplet states with the higher energy C state being odd, and the B state even. By convention, the ground state is always prefixed by X as for instance the $X^1\Sigma_g^+$ singlet state of nitrogen.

APPENDIX D

Solution of Electron Density Equation

The differential equation for electron density in the spark gap gas was given as

$$\frac{\partial n}{\partial t} + \beta n = \frac{1}{q}\left(\alpha J - \frac{\partial J}{\partial x}\right) . \tag{D-1}$$

Formally replacing $\partial x = v \partial t$; the equation becomes

$$\frac{dn}{dt} + \beta n = \frac{1}{q}\left(\alpha J - \frac{1}{v}\frac{dJ}{dt}\right) \tag{D-2}$$

where total derivatives are used because "t" is the only variable. This equation will be solved by the method of integrating factors. The equation can be written as

$$\frac{d}{dt}(\rho n) = \rho\left[\frac{1}{q}\left(\alpha J - \frac{1}{v}\frac{dJ}{dt}\right)\right] \tag{D-3}$$

if

$$\beta = \frac{1}{\rho}\frac{d\rho}{dt} \tag{D-4}$$

or

$$\rho = e^{\int^t \beta dt} = e^{\beta t} . \tag{D-5}$$

Equation (D-3) can be directly integrated,

$$\rho n = \int_0^t \rho \frac{1}{q}\left(\alpha J - \frac{1}{v}\frac{dJ}{dt}\right) dt + C . \tag{D-6}$$

Using equation (D-5) to substitute for p, equation (D-6) becomes

$$n(t) = e^{-\beta t}\int_{o}^{t} e^{\beta t}\,\frac{1}{q}\left(\alpha J - \frac{1}{v}\,\frac{dJ}{dt}\right)dt + e^{-\beta t}C \qquad \text{(D-7)}$$

where C is interpreted as an initial carrier density, n_o. Since n(t) depends on the magnitude of total current and not the direction, absolute value brackets are used in the integrand and the final solution becomes

$$n(t) = e^{-\beta t}\int_{o}^{t} e^{\beta t}\,\frac{1}{q}\left|\alpha J - \frac{1}{v}\,\frac{dJ}{dt}\right|dt + e^{-\beta t}n_o \quad . \qquad \text{(D-8)}$$

VITA

Mr. James S. Kolodzey was born on March 4, 1950 in Philadelphia, Pa. He lived with his parents, Mr. and Mrs. George Kolodzey, in Philadelphia, where he attended high school. After four years at Lehigh University, he graduated magna cum laude with a B. S. in Physics in 1972. In 1973 and 1974 he was granted a University Fellowship and became a candidate for Master of Science in Electrical Engineering.

During summer employments Mr. Kolodzey received technical experience at Teleflex Corporation and Burroughs Corporation, and is now an engineer with IBM Corporation. He is a member of the IEEE and the American Institute of Physics, and has a strong interest in optical electronics.